Persistent and anti-Persistent Motion in Bounded and Unbounded Space: Resolution of the First-Passage Problem

Daniel Marris and Luca Giuggioli

School of Engineering Mathematics and Technology, University of Bristol, BS8 1TW

E-mail: daniel.marris@bristol.ac.uk

16 April 2024

Abstract. The presence of temporal correlations in random movement trajectories is a widespread phenomenon across biological, chemical and physical systems. The ubiquity of persistent and anti-persistent motion in many natural and synthetic systems has led to a large literature on the modelling of temporally correlated movement paths. Despite the substantial body of work, little progress has been made to determine the dynamical properties of various transport related quantities, including the first-passage or first-hitting probability to one or multiple absorbing targets when space is bounded. To bridge this knowledge gap we generalise the renewal theory of first-passage and splitting probabilities to correlated discrete variables. We do so in arbitrary dimensions on a lattice for the so-called correlated or persistent random walk, the one step non-Markovian extension of the simple lattice random walk in bounded and unbounded space. We focus on bounded domains and consider both persistent and anti-persistent motion in hypercubic lattices as well as the hexagonal lattice. The discrete formalism allows us to extend the notion of the first-passage to that of the directional first-passage, whereby the walker must reach the target from a prescribed direction for a hitting event to occur. As an application to spatio-temporal observations of correlated moving cells that may be either repelled or attracted to hard surfaces, we compare the first-passage statistics to a target within a reflecting domain depending on whether an interaction with the reflective interface invokes a reversal of the movement direction or not. With strong persistence we observe multi-modality in the first-passage distribution in the former case, which instead is greatly suppressed in the latter.

1. Introduction

Advances in tracking sensors for animals [1], cells [2] and particles [3] have made conspicuous the importance of quantifying the spatio-temporal dynamics of movement. To this end, two fundamental frameworks, the lattice random walk (LRW) [4, 5, 6], and its continuous counterpart, the Brownian walk [7], have been widely employed to model and analyse Markovian trajectories, that is when the dynamics arise from history independent random processes.

Much of the versatility of the two frameworks, comes from the analytic description of diffusive processes, the quintessential example of a Markovian system. The exact mathematical representation of diffusion has in fact contributed to its widespread application across disciplines, from cell biology [8] and ecology [9] to social sciences [10] and economics [11]. However, the increased resolution of modern tracking technologies has made apparent the approximate nature of the diffusive paradigm and is highlighting the need to model accurately the non-Markovian statistics within movement paths.

One such example of non-Markovian features in spatio-temporal trajectories is persistence or anti-persistence in the movement steps, that is by having, respectively, a higher tendency to continue in the same direction or to reverse it. Although both movement statistics have been observed, persistent motion is more common and has been observed at small scales, e.g., bacteria undergoing run and tumble dynamics [12], as well as being seen at large scales, e.g., animals foraging [13] and pedestrians in dense crowds [14], while anti-persistent motion has been reported in hemocytes [15], cell extracts [16], telomeres of bone osteosarcoma cells [17] through to the evolution of the score difference in a game of basketball [18]. Persistent motion also plays a central role in the exciton coherence question [19, 20].

The ubiquity of persistent motion in many natural and artificial phenomena has generated a wealth of literature on the subject. Within the space-time continuous description much is known about the one-dimensional occupation probability [21, 5, 22, 23, 24]. However, unlike the case of Brownian walks, with correlation in the motion, the standard renewal theory approach [4, 25, 26] to find the first-passage is not sufficient to determine the temporal dependence of transport related quantities such as the first-passage or first-hitting statistics to one or multiple absorbing targets. While advances have been made in bounded space, these studies are limited to one dimension [27, 28] or can only access the mean first-passage time [29].

The main issue with a continuous spatial description in higher dimensions relates to the need to track the previous movement direction as an internal degree of freedom. In two or higher dimensions the turning angle (relative to the previous movement direction) is a continuous variable and it thus requires an infinite number of internal states [30, 31]. Moreover, as the absorption property of a target needs to be specified for each direction in which it can be reached, formalising first-passage processes in continuous space in higher dimensions remains a challenge.

By employing a discrete spatial description [4, 6] it is possible to overcome this limitation. To do that we use the so-called correlated random walk (CRW), proposed for the first time in the 1920s [32, 33], as the natural non-Markovian extension to the LRW. For the CRW, instead of prescribing a probability to move in a given direction as in the standard LRW, the movement steps are determined by the probability that the walker *continues* in the same direction as the previous step [5, 21]. In other words, with one parameter one creates persistence, or positive correlation, if the walker is more likely to continue and anti-persistence, or negative correlation, if backtracking is more likely.

Despite the long modelling history of persistent motion in the spatially discrete literature, the only major work on the CRW first-passage dynamics has appeared very recently [34]. That study considers an unbounded lattice both in one and two dimensions under the assumption that the walker moves its first step in one predetermined direction. With this simplification the one-dimensional problem may be reduced to a known first-passage quotient [35] and the exact first-passage dynamics to a single target is derived, while in two dimensions the dynamics are obtained asymptotically. Despite this recent progress, determining the general first-passage time dependence to one or multiple targets has remained an elusive task, with insights for the one target case in the bounded space relying exclusively upon studies of the global mean first-passage time in periodically bounded space [36].

In this paper, we generalise the discrete renewal equation and develop a general theory to determine the first-passage probability to a finite number of targets for a CRW in bounded and unbounded domains of arbitrary dimensions. Focusing on bounded space, we first find the analytic representation of the CRW occupation probability when space is bounded by periodic and reflective boundaries in hypercubic lattices and by periodic boundaries in a six-sided hexagonal lattice. We derive a general form of the first-passage probability and elucidate that with persistence, even in one-dimensional domains, the first-passage probability can be multi-modal. Furthermore, we extend the notion of first-passage time to the *directional* first-passage time, which we define as the probability that the walker reaches a target site from a specific direction for the first time.

As an application to flagellated bacterium that may be attracted or repelled by solid walls [37], we present an iterative process to extract occupation and first-passage probabilities with arbitrary boundary conditions. With this method we study the effect of two different reflecting boundary conditions, namely whether the boundary invokes a change of direction on various transport statistics, and show that is the former, which aids a searching walker at intermediate times.

The contents of the rest of the paper is laid out as follows. Section 2 treats the formulation of the unbounded problem. The bounded propagators or Green's function of the occupation probability in one dimensional domains are derived in Sec. 3, while their higher dimensional counterparts, together with the case of the hexagonal lattice, which we use to model chiral peristent motion, are treated in Sec. 4. In Sec. 5 we turn our attention to the placement of absorbing traps and discuss the relationship between their location and the imposition of absorbing boundary conditions on the lattice. It is here that we generalise the discrete renewal equation to correlated motion. In Sec. 6, we derive the first moments of these distributions, then in Sec. 7, we display the iterative method for calculating transport statistics for cases where the analytic solutions are not known. Concluding remarks and possible future avenues are then discussed in Sec. 8.

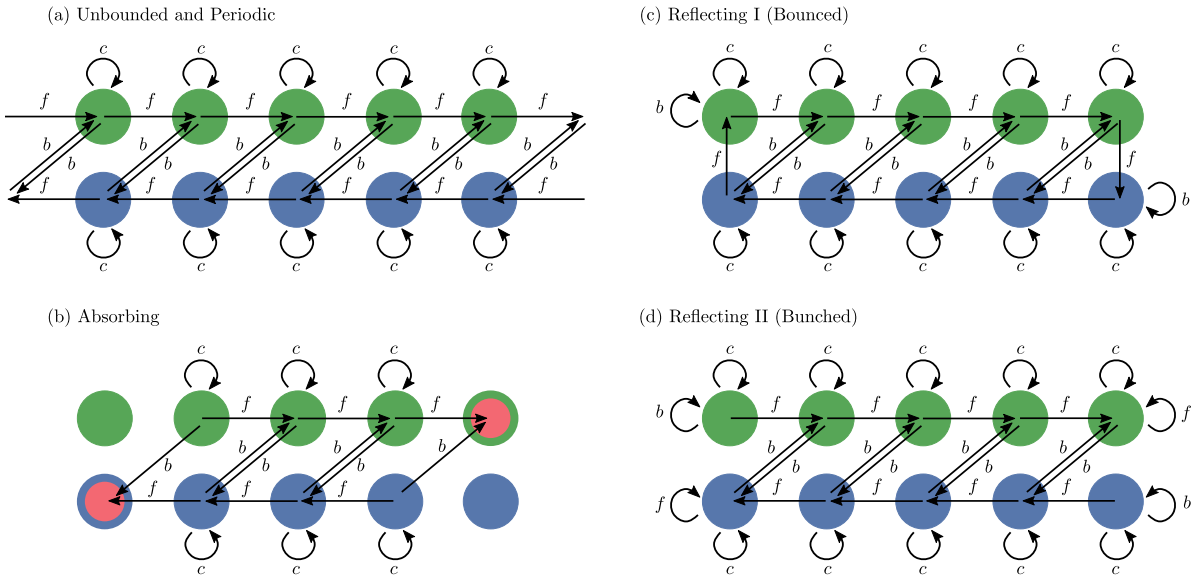

Figure 1. (Colour Online). Schematics of the two internal state representation of a persistent or anti-persistent movement process in one dimension. A spatial site consists of two states, $m = 1, 2$ shown, respectively, in green (upper circle) and blue (lower circle). Allowed steps are drawn with arrows and the parameters of their corresponding jump probabilities are shown next to the corresponding arrows. In (a), the periodic and unbounded lattices are displayed together, because the transition probabilities are identical, with the only difference arising as the wrapping between sites 1 and N in the periodic case. In panel (b) the absorbing state is drawn in red, while panels (c) and (d) represent the two types of reflection, which we label 'bounced' and 'bunched' due to the different interaction at the boundary. In the former, as a walker tries to move out of the domain, it reverses its movement direction, while in the latter it does not.

2. Unbounded Propagator

Although the CRW is a one-step non-Markov process, its dynamics can be represented by a set of coupled second-order Markov equations [38], as amply shown across the literature both in continuous [39, 24, 40] and discrete time [34]. For the latter, in one dimension it is given by

$$\begin{aligned} Q(n,1,t+1) &= fQ(n-1,1,t)+bQ(n-1,2,t)+cQ(n,1,t), \\ Q(n,2,t+1) &= bQ(n+1,1,t)+fQ(n+1,2,t)+cQ(n,2,t), \end{aligned} \tag{1}$$

where $Q(n,m,t)$ is the occupation probability at time t to be at site n and state m. The state (or internal degree of freedom) represents the direction the walker may enter the site, namely a walker in state 1 must have arrived from the left, while a walker in state 2 from the right (see schematic in Fig. 1). The parameter f is the probability of continuing forward in the direction last travelled while b is the probability of backtracking away from the previous direction travelled. $c = 1 - (f + b)$ is the so-called lazy or sojourn parameter whereby $0 < f + b \leq 1$, with $f + b = 1$ corresponding to a walker that moves at every time step. When $f > b$ the walker is in the persistent regime, while

for $f < b$ the walker is subject to anti-persistence. When $f = b$, one recovers the diffusive dynamics modelled by the LRW. The effect of the lazy parameter is akin to a rescaling of the velocity in the continuous limit of the CRW, the telegrapher's equation (see supplementary material [41] for details).

To solve Eq. (1), it is convenient to write it in matrix form as

$$\boldsymbol{Q}(n,t+1) = \mathbb{A}\cdot\boldsymbol{Q}(n-1,t) + \mathbb{B}\cdot\boldsymbol{Q}(n+1,t) + \mathbb{C}\cdot\boldsymbol{Q}(n,t), \tag{2}$$

where $\boldsymbol{Q}(n,t) = [Q(n,1,t), Q(n,2,t)]^\intercal$, $\mathbb{A} = \left[\begin{smallmatrix} f & b \\ 0 & 0 \end{smallmatrix}\right]$, $\mathbb{B} = \left[\begin{smallmatrix} 0 & 0 \\ b & f \end{smallmatrix}\right]$, and $\mathbb{C} = \left[\begin{smallmatrix} c & 0 \\ 0 & c \end{smallmatrix}\right]$ with the dot operator representing matrix multiplication.

We assume that the walker enters its initial site from the left with some arbitrary probability α_1 and from the right with $\alpha_2 = 1-\alpha_1$, such that the initial condition is written as $\boldsymbol{Q}(n,0) = \delta_{n,n_0}\boldsymbol{U_{m_0}}$ where $\boldsymbol{U_{m_0}} = [\alpha_1,\alpha_2]^\intercal$, i.e., the probability of starting in state $m_{0_1} = \alpha_1$ while the probability of starting in state $m_{0_2} = \alpha_2$, and the propagation is symmetric if $\alpha_1 = \alpha_2$. Using known procedures for random walks with internal degrees of freedom [42, 35] (outlined in Sec. II of the supplementary Material [41] for convenience), the generating function, $\widetilde{f}(z) = \sum_{t=0}^{\infty} f(t)z^t$, solution of Eq. (2), the so-called lattice Green's function or unbounded propagator, can be obtained analytically as a column vector of the occupation probability in each internal state:

$$\widetilde{\boldsymbol{Q}}_{n_0}(n,z) = \frac{1}{2\pi}\int_{-\pi}^{\pi} e^{-i\xi(n-n_0)}\left[\mathbb{I} - z\boldsymbol{\lambda}(\xi)\right]^{-1}\cdot\boldsymbol{U_{m_0}}\mathrm{d}\xi, \tag{3}$$

where $\mathbb{I}$ is the identity matrix and

$$\boldsymbol{\lambda}(\xi) = \begin{pmatrix} fe^{i\xi}+c & be^{i\xi} \\ be^{-i\xi} & fe^{-i\xi}+c \end{pmatrix}, \tag{4}$$

is the so-called structure function with ξ the Fourier variable. The (i,j)-th element of $\boldsymbol{\lambda}(\xi)$ governs the movement from state j to state i, for example, the element $\boldsymbol{\lambda}_{1,2}(\xi)$ encodes moving from state 2 to state 1, which is achieved only via a backtracking, which increases the coordinate n. $\boldsymbol{\lambda}(0)$ allows to verify the normalisation $\left(\sum_{i=1}^{2}\boldsymbol{\lambda}_{i,j}(0) = 1, j\in\{1,2\}\right)$, as expected from a stochastic matrix. The associated expression in arbitrary dimensions may be found in ref. [41], where we show a generalisation of the known unbounded propagator [43].

The integral in Eq. (3) can be evaluated exactly (see [41]), and after summing over the internal states $\widetilde{Q}(n,z) = \sum_{i=1}^{2}\widetilde{\boldsymbol{Q}}(n,z)_i$, one obtains, as a generating function, the unbounded occupation probability for the entire site as

$$\widetilde{Q}_{n_0}(n,z) = \frac{1}{(1-2cz)\sqrt{(1+\delta z^2)^2 - 4\varepsilon^2 z^2}}\left[\frac{1-cz}{r(z)^{|n-n_0|}} + \frac{\alpha_1(b-f)z}{r(z)^{|n-n_0+1|}} + \frac{\alpha_2(b-f)z}{r(z)^{|n-n_0-1|}}\right], \tag{5}$$

where $r(z) = \frac{1+\delta z^2}{2\varepsilon z}\left(1+\sqrt{1-\frac{4\varepsilon^2 z^2}{[1+\delta z^2]^2}}\right)$, $\varepsilon = f(1-cz)(1-2cz)^{-1}$ and $\delta = (f^2 - b^2 + c^2)(1-2cz)^{-1}$, and where the appearance of the higher order z terms in Eq.

(5) makes conspicuous that the system contains internal degrees of freedom. Using the relation $f + b + c = 1$, the scaling term in Eq. (5) can be rewritten as $[(1-z)[1-z(1-2b)][1-z(1-2f)]\{1-z[1-2(f+b)]\}]^{-1/2}$. In the limit $z \to 1$, as the remaining terms of Eq. (5) give the constant $2b$, we obtain $\widetilde{Q}_{n_0}(n,z) \sim b/\sqrt{2fb(f+b)(1-z)}$, alternatively the time dependence through Tauberian theorems is $Q_{n_0}(n,t) \sim b/\sqrt{2\pi fb(f+b)t}$ for $t \to \infty$. As expected, this scaling is the same as the one of the diffusive LRW, and to which it reduces when $f = b = q/2$. It is in fact a straightforward exercise to show that when $f = b$, irrespective of the values of α_1 and α_2, Eq. (5) reduces to the known solution of the symmetric unbounded walk [6].

3. Bounded Propagators

We now consider a CRW confined to a bounded domain of size N ($n \in [1, N]$) and seek the dynamics of the occupation probability in the case of periodic and reflecting boundaries. Below we use the superscript notation p and r, respectively, to distinguish them and will use the letter $\boldsymbol{P}$ to denote a bounded propagator compared to $\boldsymbol{Q}$ for the infinite case.

3.1. Periodic Boundary

For the periodic domain, the boundary condition is imposed in the same way as for the standard Pólya walk [4, 6] making it straightforward to find the periodic propagator via the method of images (see [41] Sec. III) as

$$\boldsymbol{P}^{(p)}_{n_0}(n,t) = \frac{1}{N}\sum_{\kappa=0}^{N-1} e^{\frac{-2\pi i\kappa(n-n_0)}{N}} \boldsymbol{\lambda}\left(\frac{2\pi\kappa}{N}\right)^t \cdot \boldsymbol{U_{m_0}}, \tag{6}$$

where $\boldsymbol{\lambda}(\cdot)^t$ denotes the matrix power. Diagonalising $\boldsymbol{\lambda}\left(\frac{2\pi\kappa}{N}\right)$ to take the matrix power explicitly and performing a summation over the states, one finds the site occupation probability $P^{(p)}_{n_0}(n,t) = \sum_{i=1}^{2} \boldsymbol{P}^{(p)}_{n_0}(n,t)_i$, and when $\alpha_1 = \alpha_2 = \frac{1}{2}$ we obtain

$$P^{(p)}_{n_0}(n,t) = \frac{1}{2N}\sum_{\kappa=0}^{N-1} \cos\left(\frac{2\pi\kappa(n-n_0)}{N}\right)\Big[f(\kappa,t) + h(\kappa,t)\Big], \tag{7}$$

where

$$f(\kappa,t) = \lambda_+^t + \lambda_-^t, \qquad h(\kappa,t) = \frac{b\cos\left(\frac{2\pi\kappa}{N}\right)\left[\lambda_+^t - \lambda_-^t\right]}{\sqrt{f^2\cos^2\left(\frac{2\pi\kappa}{N}\right) + b^2 - f^2}}, \tag{8}$$

and

$$\lambda_\pm = c + f\cos\left(\frac{2\pi\kappa}{N}\right) \pm \sqrt{f^2\cos^2\left(\frac{2\pi\kappa}{N}\right) + b^2 - f^2}, \tag{9}$$

are the eigenvalues of the matrix structure function $\boldsymbol{\lambda}(\frac{2\pi\kappa}{N})$. The non-symmetric case is less compact and we give it explicitly in Eq. (S23) of the supplementary material [41].

In the diffusive limit, where $f = b = \frac{q}{2}$, Eq. (6), reduces to the expression for the propagator for the LRW on a one-dimensional periodic lattice [6], while in the $f = 1$, limit one has $P_{n_0}^{(p)}(n,t) = N^{-1}\sum_{\kappa=0}^{N-1}\{\alpha_1\cos[2\pi\kappa(n-n_0+t)/N] + \alpha_2\cos[2\pi\kappa(n-n_0-t)/N]\}$, which shows a superposition of two weighted ballistic waves travelling in opposite directions. In the other limit ($b = 1$), corresponding to the perfectly anti-persistent case, the walker constantly hops between the initial condition, which it visits on even time steps, and the lattice sites on either side at odd time steps, as one may see from the resulting expression: $P_{n_0}^{(p)}(n,t) = (2N)^{-1}\sum_{\kappa=0}^{N-1}\exp[-2\pi i\kappa\,(n-n_0)\,/N]\big\{[1+(-1)^t] - [-1+(-1)^t][\alpha_1\exp(2\pi i\kappa/N) + \alpha_2\exp(-2\pi i\kappa/N)]\big\}$.

3.2. Reflective Barrier

When the correlated particle is confined within a reflecting box, there are two classes of boundary interactions that one might consider as displayed in panel (c) and (d) of Fig. 1. More specifically, one must choose whether the direction of persistence is flipped upon hitting the boundary or not. When the persistence direction is not flipped then an accumulation of particles appears at the boundary, which is reflected in the increase in the magnitude of the steady state probability at the boundary [24, 44]. We call this accumulation a 'bunching'. In contrast, when the boundary induces a change of direction, which we call a 'bounce', there is no accumulation. It is the 'bouncing' case we consider here and we find the propagator via two different methods, viz. the method of images [6] and the so-called *squeezing* method [45], which allow, respectively, for two variations on this boundary condition. We treat the 'bunched' case later in Sec. 7 and provide a comparison of the transport statistics with the 'bounced' case.

The Method of Images The method of images is a dimensionally scalable method that allows to include the effects of interfaces or boundary conditions on the walker dynamics from the knowledge of the dynamics in the absence of boundaries [46]. To account for the change in movement direction caused by a reflection, we ensure that the bounded walker changes state upon interacting with the boundary. To achieve this, one must specify boundary conditions for each internal state. More specifically, we require that $P^{(r)}(1,\{2,1\},t) = P^{(r)}(0,\{1,2\},t)$, and $P^{(r)}(N,\{1,2\},t) = P^{(r)}(N+1,\{2,1\},t)$, where the compact notation $\{i,j\}$ implies pairing the left index i (right index j), on the LHS of the equation, to the left index (right index) on the RHS. In this way, by allowing the image of state two to interact with the dynamics on state one, and vice versa, the persistent walker trying to leave the boundary will be reflected back and continue its journey in the opposite direction (see Appendix A for further discussion). With the boundary conditions set, before applying the method of images, we need to ensure that the transport process is spatially symmetric, which we accomplish by imposing $\alpha_1 = \alpha_2 = \frac{1}{2}$.

By taking the state level boundary conditions given above, and performing a

summation over the internal states, one finds the boundary condition for the entire lattice site. Upon doing so, one find the boundary condition to be $P_{n_0}^{(r)}(1,t) = P_{n_0}^{(r)}(0,t)$, $P_{n_0}^{(r)}(N,t) = P_{n_0}^{(r)}(N+1,t)$, which, as expected [47], is the same boundary condition as the diffusive random walker. Since the image set for this boundary condition has been derived recently [6], one can find the reflective propagator as $P_{n_0}^{(r)}(n,t) = \sum_{i=1}^{2} \boldsymbol{P}_{n_0}^{(r)}(n,t)_i$ where

$$\boldsymbol{P}_{n_0}^{(r)}(n,t) = \frac{1}{N}\sum_{\kappa=0}^{N-1} \beta_\kappa \cos\left(\frac{\pi\kappa(n-\frac{1}{2})}{N}\right)\cos\left(\frac{\pi\kappa(n_0-\frac{1}{2})}{N}\right)\boldsymbol{\lambda}\left(\frac{\pi\kappa}{N}\right)^t \cdot \boldsymbol{U}_{\boldsymbol{m_0}}, \tag{10}$$

with $\beta_\kappa = 1$ when $\kappa = 0$, else $\beta_\kappa = 2$ (see Sec. IV of the supplementary material [41] for a full derivation).

From Eq. (10), and similarly in Eq. (6), one may notice that, in contrast to the unbounded dynamics in Eq. (5), within periodic and reflecting domains we are able to keep separate the spatial and temporal components of the propagator. In doing so, one realises that, as expected, the respective spatial dependence in the symmetric $\alpha_1 = \alpha_2$ case coincides with the one obtained for the so-called lazy Pólya's walk in finite domains [6] and the structure function pertains in both solutions as the boundary condition does not impact the individual jump probabilities in the bulk of the domain. Since the structure of the two propagators is analogous, one can also expand Eq. (10) via the same procedure as the periodic case to find explicitly $P_{n_0}^{(r)}(n,t)$. The semi-bounded bounced propagator can also be found via the method of images and, for completeness, we have presented it in the supplementary material [41].

The Squeezing Method We exploit an alternate procedure to bound the propagator in a reflective box, which uses only the properties of the periodic propagator [45, 48, 49]. While being less scalable to higher dimensions, when compared to the method of images, it is simple to construct analytically in one-dimensional systems. This technique is particularly convenient to analyse the case when $\alpha_1 \neq \alpha_2$, since the use of an image set in a periodic geometry wraps upon itself, which avoids the interplay between the two independent image sets used to derive Eq. (10).

We follow ref. [45] and *squeeze* a torus into a reflecting lattice. More specifically, we transform a periodic domain with $M \in 2\mathbb{Z}$ sites into a reflective one with $N = (M+2)/2$ sites ($N \geq 2$) by summing the probabilities of the sites a distance l on either side of the 1^{st} and N^{th} site (see Fig. 1b in [45] or Fig. 1 of the present supplementary material [41] for a schematic representation). In doing so, we impose the boundary condition as implemented orignally by Chandrasekhar for the LRW [50], which states that the walker attempting to escape from N is bounced back to $N-1$ with certainty, and similarly for site $n = 1$. The reflective propagator with this condition is [45]

$$\boldsymbol{P}_{n_0}^{(r_s)}(n,t) = \boldsymbol{P}_{n_0}^{(p)}(n,t) + \mu(n)\boldsymbol{P}_{n_0}^{(p)}(M+2-n,t), \tag{11}$$

where we indicate with the superscript r_s that the reflecting domain has been accounted by squeezing a periodic one, and where $\mu(n) = 0$ when $n = 1$ or N, and $\mu(n) = 1$,

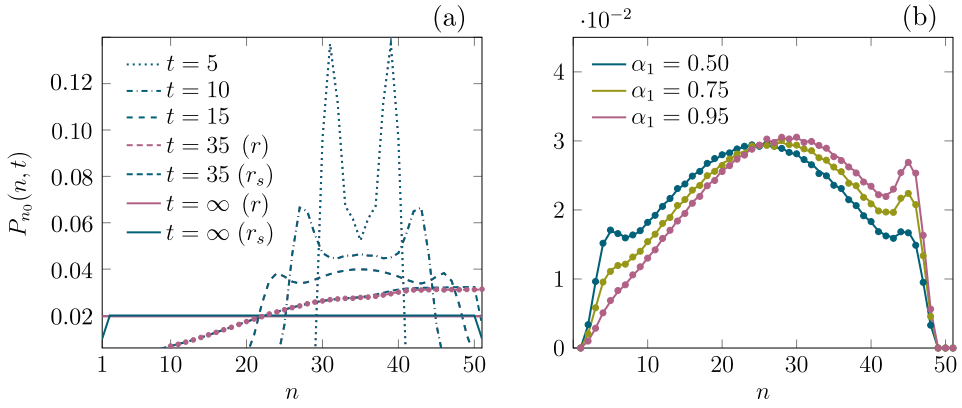

Figure 2. (Colour Online). The occupation probability in a one-dimensional reflecting domain of length $N = 51$ found via the method of images, Eq. (10), and the squeezing technique, Eq. (12). Panel (a) shows the evolution of the occupation probability of both propagators, with the method of images (r) solution plotted in purple and the squeezed solution (r_s) displayed in blue, for the symmetric $\alpha_1 = \alpha_2 = 0.5$ case. For clarity, as there is no differences between the dynamics of the two propagators before boundary interaction, we omit in the legend the entries for the method of images solution at short times. The dynamics seen are with $f = 0.7$, $b = 0.1$ and $n_0 = 35$. Panel (b) depicts the occupation probability of the squeezed propagator at $t = 23$ with $n_0 = 25$, $f = 0.8$, $b = 0.1$. Here we examine the effect of changing α_1 and $\alpha_2 = 1 - \alpha_1$. The dots on some curves across the two panels represent the ensemble average of 10^6 stochastic simulations.

otherwise. We note that by construction, in this instance, one should not think of the states as being representative of the direction of motion previously travelled, since the baseline propagator on the torus, from which Eq. (11) is built, considers trajectories that may enter each lattice site from either direction.

Using Eqs. (6) and (11), and after some algebra, the reflective propagator is given explicitly by

$$\boldsymbol{P}_{n_0}^{(r_s)}(n,t) = \frac{1}{2N-2}\sum_{\kappa=0}^{2N-3}\left[\exp\left(\frac{-\pi i\kappa(n-n_0)}{N-1}\right) + \mu(n)\exp\left(\frac{-\pi i\kappa(2N-n-n_0)}{N-1}\right)\right]\boldsymbol{\lambda}\left(\frac{\pi\kappa}{N-1}\right)^t \cdot \boldsymbol{U}_{\boldsymbol{m_0}}. \tag{12}$$

In Fig. 2(a), we plot the reflecting propagator found via both methods (Eqs. (10) and (12)). For times small enough that no boundary interaction has occurred, one cannot distinguish between the two representations, as expected. However, after boundary interaction, the occupation probability differs slightly due to the no-waiting scheme at the boundary that Eq. (12) obeys. Since these sites can be viewed as 'slippy', i.e., the chance of leaving the site is higher than the rest of the domain, the steady state distribution shows a bench-like structure, with these boundary sites having a lower probability of being occupied. In fact, it can be shown (see Appendix B) that when f and b are not identically one, $P_{n_0}^{(r_s)}(n, t \to \infty) = \frac{1}{(N-1)}$ $(n \neq \{1, N\})$ while

$P_{n_0}^{(r_s)}(1, t\to\infty) = P_{n_0}^{(r_s)}(N, t\to\infty) = \frac{1}{2(N-1)}$.

In Fig. 2(b), we display the effect of the weightings over the internal states in the initial condition. When $\alpha_1 \neq \alpha_2$, the propagation is clearly asymmetric, as the higher weighting of trajectories that started right are likely to continue heading right.

4. Propagators in Higher Dimensions

As mentioned in the introduction, in continuous space modelling persistence in higher dimensions requires the inclusion of an infinite number of internal variables [30]. A discrete representation, on the other hand, requires only Z internal variables, where Z is the coordination number of the lattice. In dimensions larger than one, we require a third parameter, ℓ, to govern the probability of turning, which we define as a change of movement direction in any direction except turning back. For simplicity, we first assume the probability of moving in any lateral direction, to be uniform, although this can be relaxed with no additional mathematical burden, as we will show below with the hexagonal lattice. Moreover, in the d dimensional hypercubic lattice we demand $f + b + \mathfrak{d}\ell + c^{(\mathfrak{d})} = 1$, where $\mathfrak{d}$ is the number of permissible lateral movements, defined as $\mathfrak{d} = Z - 2$ and $c^{(\mathfrak{d})}$ is the sojourn probability. The initial condition must also account for the higher number of movement directions, meaning that $\boldsymbol{Q}_{\boldsymbol{n}_0}(\boldsymbol{n}, 0) = \prod_{i=1}^{d}\left(\delta_{n_i,n_{0_i}}\right)\boldsymbol{U}_{\boldsymbol{m}_0}$, where $\boldsymbol{U}_{\boldsymbol{m}_0} = [\alpha_1, ..., \alpha_{2d}]^\intercal$.

4.1. Hypercubic Lattices

We again start by writing a Master equation to govern the unbounded dynamics. In d dimensions, this takes the form of $2d$ coupled equations, which we have written explicitly for the $d = 2$ case in the supplementary material [41]. Akin to the $d = 1$ case, it is convenient to re-write the coupled equations in matrix form, and for arbitrary dimension d, we obtain

$$Q(\boldsymbol{n}, t+1) = \sum_{i=1}^{d}\left\{\mathbb{A}_{2d}^{(i)}\cdot Q(\boldsymbol{n}-\boldsymbol{e}_i, t)+\mathbb{B}_{2d}^{(i)}\cdot Q(\boldsymbol{n}+\boldsymbol{e}_i, t)\right\} + \mathbb{C}_{2d}\cdot Q(\boldsymbol{n}, t), \tag{13}$$

where $\boldsymbol{e}_i$ is a unit vector along dimension i. $\mathbb{A}_{2d}^{(i)}$, $\mathbb{B}_{2d}^{(i)}$ are $2d\times 2d$ matrices that govern the movement probabilities along either direction of the i^{th} axis, which is encoded via elements along $(2i-1)^{\text{th}}$ and $2i^{\text{th}}$ rows, respectively, while all other rows in $\mathbb{A}_{2d}^{(i)}$ and $\mathbb{B}_{2d}^{(i)}$ are identically zero. $\mathbb{C}_{2d}$ governs the sojourn probability and is of the form $\mathbb{C}_{2d} = c^{(\mathfrak{d})}\mathbb{I}$.

The method of images allows us to find the periodic and reflective propagator in arbitrary dimensions. Following the supplementary material [41], we find the propagator in arbitrary dimensions again as a summation of column vector of state probabilities $P_{n_{01},...,n_{0d}}^{(\gamma)}(n_1, ..., n_d, t) = \sum_{m=1}^{2d}\boldsymbol{P}_{n_{01},...,n_{0d}}^{(\gamma)}(n_1, ..., n_d, t)_m$, where

$$\boldsymbol{P}^{(\gamma)}_{n_{01},...,n_{0d}}(n_1,...,n_d,t)=\frac{1}{N^d}\sum_{\kappa_1=0}^{N_1-1}...\sum_{\kappa_d=0}^{N_d-1}\left[\prod_{i=1}^{d}g^{(\gamma)}_{\kappa_i}(n_i,n_{0_i})\right]\boldsymbol{\lambda}\left(\pi\mathcal{N}^{(\gamma)}_{\kappa_1},...,\pi\mathcal{N}^{(\gamma)}_{\kappa_d}\right)^t\cdot\boldsymbol{U}_{\boldsymbol{m}_0}, \tag{14}$$

and $\gamma = p$ or r. The function $g^{(\gamma)}_{\kappa_i}(n_i,n_{0_i})$ is the spatial dependence of the periodic or reflective bounded domain, given by $g^{(p)}_{\kappa_j}(n_j,n_{0_j}) = \exp[-2\pi i\kappa_j(n_j-n_{0_j})/N_j]$ and $g^{(r)}_{\kappa_j}(n_j,n_{0_j}) = \beta_{\kappa_j}\cos[\pi\kappa_j(n_j-1)/(N_j)]\cos[\pi\kappa_j(n_{0_j}-1)/(N_j)]$, and where $\mathcal{N}^{(p)}_i = 2\kappa_i/N_i$, while $\mathcal{N}^{(r)}_i = \kappa_i/N_i$. We note that, similarly to the $d = 1$ case, the image method demands that when $\gamma = r$ the initial weighting over the states to be uniform.

The $2d\times 2d$ matrix $\boldsymbol{\lambda}\left(\pi\mathcal{N}^{(\gamma)}_{\kappa_1},...,\pi\mathcal{N}^{(\gamma)}_{\kappa_d}\right)$ maintains a simple structure regardless of the dimension and also allows straight forward calculation of the uniform steady state for both $\gamma = p$ or r (see Appendix B). Explicit analytical expressions of the scalar propagator for the site occupation probability depends on the analytical determination of the eigensystem of $\boldsymbol{\lambda}\left(\pi\mathcal{N}^{(\gamma)}_{\kappa_1},...,\pi\mathcal{N}^{(\gamma)}_{\kappa_d}\right)$. We discuss some of these analytic cases starting from the fully correlated or anti-correlated limits. In those cases many elements of $\boldsymbol{\lambda}\left(\pi\mathcal{N}^{(\gamma)}_{\kappa_1},...,\pi\mathcal{N}^{(\gamma)}_{\kappa_d}\right)$ reduce to zero. When $b,\ell = 0$, the matrix is diagonal, so it is trivial to take the matrix power explicitly and the propagator is simply the sum of the matrix diagonal elements weighted according to $\boldsymbol{U}_{\boldsymbol{m}_0}$. Furthermore, when $f,c,\ell = 0$, the structure function reduces to a generalised permutation matrix, which one may also take to arbitrary power in closed form.

As $\sum_{t=0}^{\infty} z^t\boldsymbol{\lambda}(\cdot)^t = [\mathbb{I}-z\boldsymbol{\lambda}(\cdot)]^{-1}$ in employing generating functions, it may become more convenient to take a matrix inverse than calculating the eigensystem to determine the propagator in time. To illustrate this aspect, we consider the simplified cases discussed in [51, 36], whereby the authors make the assumption that the probability of a lateral movement is equivalent to that of a backward movement, which corresponds to setting $b = \ell$ in our notation. We display the generating function of the occupation probability for this case in Sec. V of ref. [41].

Furthermore, carrying out the same procedure, but now setting $f = \ell$, one obtains a structure function matrix where the eigenvalues can be calculated explicitly (see [41]). Following this, the propagator for the entire site probability can in fact be determined in the time domain as

$$\widetilde{P}^{(\gamma)}_{n_{0_1},n_{0_2}}(n_1,n_2,t) = \frac{1}{2N^2}\sum_{\kappa_1=0}^{N-1}\sum_{\kappa_2=0}^{N-1}\left[\prod_{i=1}^{2}g^{(\gamma)}_{\kappa_i}(n_i,n_{0_i})\right]\left[f(\kappa_1,\kappa_2,t)+\frac{1-2\ell}{2\ell}g(\kappa_1,\kappa_2,t)\right], \tag{15}$$

where

$$f(\kappa_1,\kappa_2,t) = \psi_+(\kappa_1,\kappa_2)^t+\psi_-(\kappa_1,\kappa_2)^t, \tag{16}$$

$$g(\kappa_1,\kappa_2,t) = \frac{\sigma(\kappa_1,\kappa_2)\left[\psi_+(\kappa_1,\kappa_2)^t-\psi_-(\kappa_1,\kappa_2)^t\right]}{\sqrt{\sigma(\kappa_1,\kappa_2)^2+1-4\ell}}, \tag{17}$$

$$\psi_{\pm}(\kappa_1, \kappa_2) = \sigma(\kappa_1, \kappa_2) \pm \sqrt{\sigma(\kappa_1, \kappa_2)^2 + 1 - 4\ell}, \tag{18}$$

and

$$\sigma(\kappa_1, \kappa_2) = \ell \left(\cos\left[\pi \mathcal{N}_{\kappa_1}^{(\gamma)}\right] + \cos\left[\pi \mathcal{N}_{\kappa_2}^{(\gamma)}\right] \right). \tag{19}$$

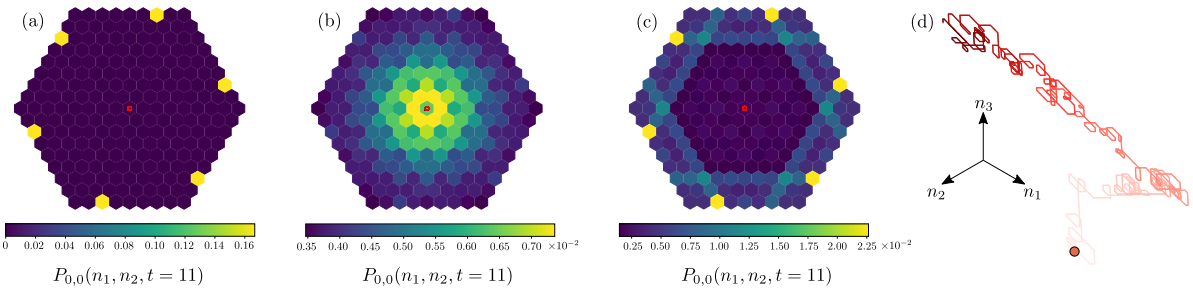

Figure 3. (Colour Online). Correlated motion in hexagonal lattices. Panels (a)-(c) show the occupation probability from Eq. (20) at time $t = 11$ in a hexagonal domain with circumradius $R = 8$ ($\Omega = 217$) and initial condition at the origin (shown via the red circles) with $\boldsymbol{U_{m_0}} = (1, 1, 1, 1, 1, 1)^{\intercal}/6$. The boundary condition is taken as the right-shift periodic boundary condition, and we provide further details of how this impacts the dynamics in ref. [41]. In panel (a) the walker is ballistic ($f = 1$) and there is no steady state. There are instead probability pulses of magnitude $\frac{1}{6}$ that travel around the domain for all time. In panel (b) $f = 0.6$, $b = 0.06$ and $\ell_{\{1,2,3,4\}} = 0.085$, while in panel (c) $f = 0.8$, $\ell_1 = 0.2$ ($b = \ell_{\{2,3,4\}} = 0$). Panel (d) depicts a sample trajectory, with the same movement probabilities as panel (c). The trajectory is over 2000 timesteps and the colour of the trajectory indicates the time, with light red indicating short times and dark red indicating long times. The domain is of size $R = 700$, which is chosen so the walker does not interact with the boundary, and we omit the boundary for visual ease. The initial condition is shown by the orange circle at (0,0,0) and the coordinate axes for the hexagonal lattice are shown via the black arrows.

4.2. Hexagonal Lattice

There has been some attempts in the past to study correlated motion in a hexagonal setting. The steady state of a run and tumble model which can change direction by a rotation of 60° was studied analytically in [52], while the path of a persistent photon with varying angles of incidence is studied as a 12^{th} order Markov chain in a reflecting hexagonal geometry in [53], where long time diffusion constants and moments are derived. Moreover, the CRW on a hexagonal lattice has been used in [13] to determine optimal search strategies for central place foragers.

When considering the hexagonal lattice, it is convenient to use Her's three axis coordinate system [54] where each coordinate is represented by three linearly dependent coordinates (n_1, n_2, n_3) such that $n_1 + n_2 + n_3 = 0$. The finite domain is six-sided, with the number of lattice points $\Omega = 3R^2 + 3R + 1$ governed by the circumradius of the hexagon R. As the coordination number in this case is $Z = 6$, we require

$f + b + \sum_{j=1}^{4} \ell_j + c^{(4)} = 1$ and $\boldsymbol{U}_{\boldsymbol{m}_0}$ is a 6×1 column vector. Each lateral movement direction is defined in relation to the previous movement step where ℓ_1 governs the probability of a 60° rotation anticlockwise, ℓ_2 a 120° anticlockwise rotation, ℓ_3 a 120° clockwise rotation and ℓ_4 that of a 60° clockwise rotation (see [41] (Fig. 2) for pictorial representation). With these parameters, we find the propagator for correlated motion in a periodic hexagonal geometry as (see [41])

$$\boldsymbol{P}_{\boldsymbol{n}_0}^{(\mathcal{H})}(\boldsymbol{n}, t) = \Bigg\{ \frac{\boldsymbol{\lambda}^{(\mathcal{H})}(0,0)^t}{\Omega} + \frac{1}{\Omega} \sum_{r=0}^{R-1} \sum_{s=0}^{3r+2} e^{\frac{2\pi i \boldsymbol{\kappa}\cdot(\boldsymbol{n}-\boldsymbol{n}_0)}{\Omega}} \boldsymbol{\lambda}^{(\mathcal{H})}\big(\boldsymbol{\kappa}(r,s)\big)^t + e^{\frac{-2\pi i \boldsymbol{\kappa}\cdot(\boldsymbol{n}-\boldsymbol{n}_0)}{\Omega}} \boldsymbol{\lambda}^{(\mathcal{H})}\big(-\boldsymbol{\kappa}(r,s)\big)^t \Bigg\} \cdot \boldsymbol{U}_{\boldsymbol{m}_0}, \tag{20}$$

with the vector $\boldsymbol{\kappa}(r,s) = 2\pi[\kappa_1(r,s), \kappa_2(r,s)]/\Omega$ having components $\kappa_1(r,s) = R(s+1) + s - r$ and $\kappa_2(r,s) = R(2 - s + 3r) + r + 1$ [55] and with $\boldsymbol{\lambda}^{(\mathcal{H})}(\cdot,\cdot)$ defined in Eq. (S45) of the supplementary material [41].

In a periodic hexagon the non-orthogonality of the coordinates leads to a shift as the walker crosses the domain boundaries [55]. In the context of this present work, if a ballistic walker traverses across the upper boundary it will continue its path via the bottom edge, but shifted along one coordinate. One can choose which way to shift the walker, and we have arbitrarily chosen the right shift here. For such a case, in Fig. 3(a), we display the probability when the dynamics are ballistic, where one observes pulses of probability with magnitude 1/6, which originally travelled from the origin to the six corners, have traversed the boundary and are no longer on their original axis. Since each side of the hexagon is shifted in the same way, the rotational symmetry remains, which is also seen in a less persistent case in panel (b).

An interesting feature of this boundary condition is that the ballistic walker in the periodic hexagonal lattice is guaranteed to visit every site, which we show mathematically in Sec. VI of the supplementary material [41]. In contrast, in the square lattice, either periodic or reflecting, the ballistic walker is confined to a genuine sublattice, i.e. only the coordinates $[(1, n_{0_2}), ..., (N, n_{0_2}), (n_{0_1}, 1), ..., (n_{0_2}, N)]$, which can be evinced as when b and s are identically zero, $\left[\mathbb{I} - \boldsymbol{\lambda}\left(\pi\mathcal{N}_{\kappa_1}^{(\gamma)}, \pi\mathcal{N}_{\kappa_2}^{(\gamma)}\right)\right]^{-1}$ is singular away from $\kappa_1 = \kappa_2 = 0$, which occurs only when the walk is confined to a genuine sublattice [56]. This has interesting implications on the search time of the walkers in these lattices. Clearly, when the target is away from the coordinates of the sublattice, the search time of the walker in the square lattice becomes increasingly longer as persistence is increased [36] until the probability of a first-passage event ever taking place becomes zero. However, on the hexagonal lattice, the ballistic walker will, with probability one, hit the target in $t \leq \Omega$ timesteps making an increase of persistence a good search strategy with the periodic hexagonal boundary condition.

Chiral Motion By relaxing the assumption that all lateral movement directions are uniformly distributed, we introduce the possibility of looping patterns into the

movement. We present this as a discrete alternative to the model of 'chiral' persistent motion [30, 57, 58, 59], where an angular bias is introduced into the turning angle, which is of interest as a model of a charged particle subjected to soft scattering by aligned magnetic domains [30] and particles driven by microscopic torques such as active colloids [60] and spermatozoa [61], and chlamydomonas [62]. While chiral motion appears at first to lend itself to a continuous space representation, it is known that even the two-dimensional case leads to an analytical intractable Fokker-Planck equation [30], meaning occupation probabilities and further transport quantities are difficult to obtain. On the other hand, in the discrete paradigm, to create looping, one merely alters the movement probabilities in $\boldsymbol{\lambda}^{(\mathcal{H})}(\cdot,\cdot)$ allowing to obtain with ease the occupation probability.

We create this motion, with anti-clockwise loops, by first setting $c^{(4)} = 0$ and then $f, \ell_1 > b, \ell_{\{2,3,4\}}$, i.e. the probability of either continuing forward or turning 60° is much larger than any other movement direction. For this chiral example, using the parameters $f = 0.8$, $\ell_1 = 0.2$, we plot the occupation probability in Fig. 3(c) and a sample trajectory in Fig. 3(d) in a large domain so that no boundary interaction takes place. The single trajectory displays periods of persistent motion before making loopy turns, which are anti-clockwise in most cases. To control these loops, one may either employ a larger ℓ_1, while decreasing f, so that their frequency increases, or one may increase ℓ_2 at the expense of ℓ_1, to tighten loops. To create clockwise loops, one instead places the turning probability into ℓ_3 or ℓ_4 instead.

5. Absorbing Traps and First-Passage Processes

In the presence of absorbing traps, the one-dimensional boundaries to be imposed on the equation governing the occupation probability for the persistent random walk are known [39]. As shown pictorially in Fig. 1(b) for the one dimensional case, to constrain entirely the domain between sites $n = 1$ and $n = N$, the Master equation needs to satisfy the boundary condition $P^{(a)}(N, 1, t) = P^{(a)}(1, 2, t) = 0$, where now the superscript a indicates the presence of absorbing boundaries.

In two and higher dimensions, the constraints to represent a fully absorbing domain can be understood by considering, for simplicity, the square lattice. Here, with $Z = 4$ the states 1,2,3 and 4 represent, respectively, a walker that has moved West, East, North and South in the last movement step. In this case, the walker can reach the West of the domain only by increasing its n_1 coordinate, thus reaching any site with coordinate $n_1 = N$ in state 1, the north of the domain by increasing its n_2 coordinate, thus reaching site $n_2 = N$ in state 3, etc. As such, there is only one movement direction the walker can undertake which results in an absorption at each boundary, leading to the boundary condition $P^{(a)}(N, n_2, 1, t) = P^{(a)}(1, n_2, 2, t) = P^{(a)}(n_1, N, 3, t) = P^{(a)}(n_1, 1, 4, t) = 0$. One may extend this logic to any lattice, that is, to create a fully absorbing boundary traps need to be placed in only the one state in each of the boundary sites that corresponds to the movement direction into that boundary.

On the other hand, in the cases when the traps are not complete along the

domain boundaries, are partially absorbing, or more generally, when traps are away from boundary sites, one needs to consider all the states in a site to make it fully absorbing. To do that one must choose an appropriate absorption free propagator. While the method of images solution in a periodic domain is amenable to placing traps, the reflective method of images solution is hardly useful when extracting first-passage distributions. To explain why, recall, as shown in Sec. 3.2 (and Appendix A), that the construction of the reflective propagator is reliant on the interplay between the symmetric propagation in state one (two) and its oppposite image in state two (one). Hence, once a trap is placed on an individual state, which stops movement along one direction, the dynamics with the trap in site one (two) is no longer symmetric with its image counterpart representing movement along state two (one). To overcome this issue, in this Section we use the squeezed propagator viz. Eq. (10), for the reflective occupation probability, which requires no symmetry between individual image sets, since it is built using periodic propagators.

We are interested in studying first-passage processes both when a single target consists of a subset of the $i = 1, ..., M$ internal degrees of freedom or all of them (the entire site), in the cases where the initial probability is shared between any or all of the internal states in $\boldsymbol{n}_0$. Since the set of trajectories that originate in state $\boldsymbol{n}_0, m_i$ are independent of those starting in $\boldsymbol{n}_0, m_j$ and those terminating in $\boldsymbol{s}, m_{\boldsymbol{s}_i}$ are independent of those terminating in $\boldsymbol{s}, m_{\boldsymbol{s}_j}$ $(i \neq j)$, it suffices to consider them separately and sum the result. Furthermore, when there are multiple targets, the summation is carried out over both the internal states and the site location.

In the presence of an unordered set of absorbing traps $\mathcal{S} = \{(\boldsymbol{s}, m_{\boldsymbol{s}})_i, ..., (\boldsymbol{s}, m_{\boldsymbol{s}})_S\}$ (S is the cardinality of the set), where each element represents a trap in the internal state at $(\boldsymbol{s}_i, m_{\boldsymbol{s}_i})$, we obtain (see Appendix C for the details) the following propagator generating function

$$\widetilde{P}^{(a)}_{\boldsymbol{n}_0}(\boldsymbol{n}, z) = \widetilde{P}_{\boldsymbol{n}_0}(\boldsymbol{n}, z) - \sum_{m=1}^{M}\sum_{j=1}^{M}\sum_{i=1}^{S} \alpha_{m_{\boldsymbol{s}_i}} \widetilde{P}_{\boldsymbol{s},m_{\boldsymbol{s}_i}}(\boldsymbol{n}, m, z) \frac{\det[\mathbb{H}^{(i)}(\boldsymbol{n}_0, m_{0_j}, z)]}{\det[\mathbb{H}(z)]}, \tag{21}$$

where $\mathbb{H}(z)_{l,k} = \alpha_{m_{\boldsymbol{s}_k}} \widetilde{P}_{\boldsymbol{s}_k,m_{\boldsymbol{s}_k}}(\boldsymbol{s}_l, m_{\boldsymbol{s}_l}, z)$, $\mathbb{H}(z)_{k,k} = \alpha_{m_{\boldsymbol{s}_k}} \widetilde{P}_{\boldsymbol{s}_k,m_{\boldsymbol{s}_k}}(\boldsymbol{s}_k, m_{\boldsymbol{s}_k}, z)$ and $\mathbb{H}^{(i)}(\boldsymbol{n}_0, m_0, z)$ is the same, but with the i^{th} column replaced with $\alpha_{m_{0_j}} \left[\widetilde{P}_{\boldsymbol{n}_0,m_{0_j}}(\boldsymbol{s}_1, m_{\boldsymbol{s}_1}, z), ..., \widetilde{P}_{\boldsymbol{n}_0,m_{0_j}}(\boldsymbol{s}_S, m_{\boldsymbol{s}_S}, z)\right]^{\intercal}$. The notation $\alpha_{m_{0_j}} P_{\boldsymbol{n}_0,m_{0_j}}(\boldsymbol{n}, m, t) = \alpha_{m_{0_j}} \boldsymbol{e}^{\intercal}_m \cdot \boldsymbol{P}_{\boldsymbol{n}_0}(\boldsymbol{n}, t) \cdot \boldsymbol{e}_{m_{0_j}}$, is the occupation probability that the walker occupies site and state $(\boldsymbol{n}, m)$ given its initial position was $(\boldsymbol{n}_0, m_{0_j})$, which is weighted by $\alpha_{m_{0_j}}$.

To help elucidate the notation we note that while the site-state pair defining the trap location is unique, it is possible to have multiple states within one site containing traps. For example, consider the case of a fully absorbing trap in site $\boldsymbol{s}$ in a two-dimensional square lattice. Since a trap in state $m_{\boldsymbol{s}} = 1$ of site $\boldsymbol{s}$ absorbs a walker reaching $\boldsymbol{s}$ from the left (movement along the West direction) only, traps must also be placed in sites $m_{\boldsymbol{s}} = 2, 3$ and 4 to absorb a walker entering the site from any direction. Hence, for this case $\mathcal{S} = \{(\boldsymbol{s}, 1), (\boldsymbol{s}, 2), (\boldsymbol{s}, 3), (\boldsymbol{s}, 4)\}$.

First-Passage and Splitting Dynamics

Knowledge of the occupation probability for the absorbing propagator allows us to study other transport statistics such as the first exit or first-passage time [25, 26]. By performing a spatial summation, we find the generating function of the survival probability, namely $\widetilde{S}_{\boldsymbol{n}_0}(z) = \sum_{\boldsymbol{n}} \widetilde{P}^{(a)}_{\boldsymbol{n}_0}(\boldsymbol{n}, z)$, and from the known relation $\widetilde{F}_{\boldsymbol{n}_0}(\boldsymbol{n}, z) = 1 - (1-z)\widetilde{S}_{\boldsymbol{n}_0}(z)$, we obtain the generating function for the first-passage probability to an arbitrary number of target states as

$$\widetilde{F}_{\boldsymbol{n}_0}(\mathcal{S}, z) = \sum_{j=1}^{M}\sum_{i=1}^{S} \alpha_{m_{\boldsymbol{s}_i}} \frac{\det[\mathbb{H}^{(i)}(\boldsymbol{n}_0, m_{0_j}, z)]}{\det[\mathbb{H}(z)]}. \tag{22}$$

With multiple targets ($S > 1$), the theory also allows the determination of the so-called splitting probability, that is the probability of reaching $\boldsymbol{s}_k$ and not any of the other targets in $\mathcal{S}$. Following ref. [63], one finds

$$\widetilde{F}_{\boldsymbol{n}_0}(\boldsymbol{s}_k|\boldsymbol{s}_1; ...; \boldsymbol{s}_k - 1; \boldsymbol{s}_k + 1; ...; \boldsymbol{s}_S, z) = \alpha_{m_{\boldsymbol{s}_k}} \frac{\sum_{j=1}^{M} \det[\mathbb{H}^{(k)}(\boldsymbol{n}_0, m_{0_j}, z)]}{\det[\mathbb{H}(z)]}. \tag{23}$$

Equations (22) and (23) are the sought-after quantities. They are the solution for the multi-target first-passage and splitting problems, respectively, for random walks with internal degrees of freedom, of which the focus of this study, the CRW, is one such example. The expressions are general and accounts for an arbitrary distribution over $\boldsymbol{U}_{\boldsymbol{m}_0}$ with any number of target states, which may be located in one or multiple lattice sites.

Depending on the problem Eq. (22) can be simplified to more compact expressions. The simplest case is the one target state for the one-dimensional unbounded CRW. In such a scenario, if the target state is located at site $s > n_0$, one may put the target at $(s, 1)$ since the walker may only arrive at s from the left, as one can evince by looking at Fig. 1(b). With a single target state, Eq. (22) can be written as

$$\widetilde{F}_{\boldsymbol{n}_0, m_0}(\boldsymbol{s}, m_{\boldsymbol{s}}, z) = \frac{\sum_{j=1}^{M} \alpha_{m_{0_j}} \widetilde{P}_{n_0, m_{0_j}}(\boldsymbol{s}, m_{\boldsymbol{s}}, z)}{\widetilde{P}_{\boldsymbol{s}, m_{\boldsymbol{s}}}(\boldsymbol{s}, m_{\boldsymbol{s}}, z)}, \tag{24}$$

which can be further reduced to the known first-passage quotient for random walks with internal degrees of freedom $\widetilde{F}_{\boldsymbol{n}_0, m_{0_k}}(\boldsymbol{s}, m_{\boldsymbol{s}}, z) = \frac{\widetilde{P}_{\boldsymbol{n}_0, m_{0_k}}(\boldsymbol{s}, m_{\boldsymbol{s}}, z)}{\widetilde{P}_{\boldsymbol{s}, m_{\boldsymbol{s}}}(\boldsymbol{s}, m_{\boldsymbol{s}}, z)}$ [35, 34] when the initial condition is localised at state m_{0_k}.

For the bounded one-dimensional lattice, where the walker may enter from either direction, the case with two target states at the same spatial site, e.g., $\mathcal{S} = \{(s, 1), (s, 2)\}$, is particularly relevant. Here, Eq. (22) can be expanded out (see Sec. VII of ref. [41])

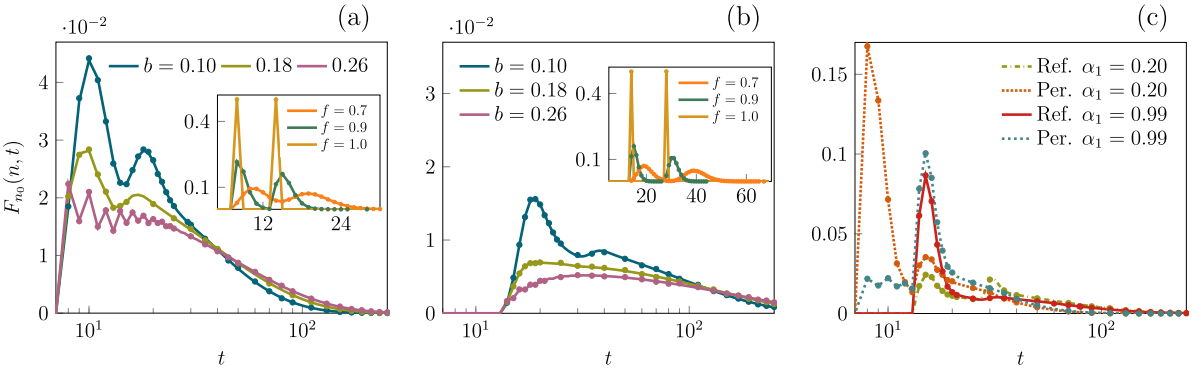

Figure 4. (Colour Online). First-passage probability in a finite one dimensional domain of size $N = 22$ with initial condition $n_0 = 8$ and a target at $s = N$ obtained via a numerical z-inverse transform [64, 65] of Eq. (25), with the periodic propagator, Eq. (6), used for panel (a) and the squeezed reflective propagator, Eq. (12), used for panel (b). We note here the use of the two state first-passage in the squeezed reflective propagator is needed as it is constructed via the periodic dynamics. In the main figure of panel (a) and (b) we use $\alpha_1 = \alpha_2 = 1/2$, $f = 0.65$ and we vary b, while in the insets we set $b = 0$ and vary f. In (c) we fix $f = 0.82$, $b = 0.08$ and study how the first-passage probability changes as we change α_1. The lines are again obtained from Eq. (25) with the appropriate propagator. Across all three panels the dots represent the ensemble average of 10^6 stochastic simulations.

to find

$$\widetilde{F}_{n_0}(s,z) = \frac{\alpha_1\Big(\widetilde{P}_{n_0,1}(s,1,z)\left[\widetilde{P}_{s,2}(s,2,z)-\widetilde{P}_{s,1}(s,2,z)\right]+\widetilde{P}_{n_0,1}(s,2,z)\left[\widetilde{P}_{s,1}(s,1,z)-\widetilde{P}_{s,2}(s,1,z)\right]\Big)}{\widetilde{P}_{s,1}(s,1,z)\widetilde{P}_{s,2}(s,2,z)-\widetilde{P}_{s,1}(s,2,z)\widetilde{P}_{s,2}(s,1,z)} + \frac{\alpha_2\Big(\widetilde{P}_{n_0,2}(s,1,z)\left[\widetilde{P}_{s,2}(s,2,z)-\widetilde{P}_{s,1}(s,2,z)\right]+\widetilde{P}_{n_0,2}(s,2,z)\left[\widetilde{P}_{s,1}(s,1,z)-\widetilde{P}_{s,2}(s,1,z)\right]\Big)}{\widetilde{P}_{s,1}(s,1,z)\widetilde{P}_{s,2}(s,2,z)-\widetilde{P}_{s,1}(s,2,z)\widetilde{P}_{s,2}(s,1,z)}, \tag{25}$$

where we have lightened the notation with $\widetilde{F}_{n_0}(s,z) = \widetilde{F}_{n_0}(\{(s,1),(s,2)\},z)$, $\alpha_{m_{0_1}} = \alpha_1$ and similarly for the second state weighting. The alternative derivation via a generalised renewal equation of Eqs. (24) and (25) can be found in Sec. VII of ref. [41].

A prominent feature of the first-passage probability for a bounded CRW is the appearance of multiple peaks. While in periodic domains bi-modal [66, 67, 68] and multi-modal [69] first-passage distributions for Markov LRWs have been reported, in those cases the appearance of multiple peaks is a consequence of the periodicity of the boundaries and the presence of a bias for which there are repeated occasions when a fraction of the trajectories may hit a target. This is not the case for the CRW, as we observe multiple peaks with periodic as well as reflecting domains.

With correlated motion we may in fact identify trajectories that travel both towards and away from the target. With the existence of two peaks documented in Fig. 4, the

first peak corresponds to those trajectories, which travel persistently towards the target and the second peak represents those that travel away and later come back via, either, a bouncing reflection or the periodic boundary. Since the peaks correspond to the two sets of trajectories, the initial weighting controls which peak contains larger probability, while the overall level of persistence governs their collective height. Furthermore, for a given domain size, the path that reaches the target via the periodic boundary is always shorter than the path that bounces back via the reflective boundary. Hence, the time at which the second peak occurs is always lower in periodic domains when compared to its reflective counterpart, which may also be seen by comparing panels (a) and (b).

In panel (c), the effect of the individual weighting on the height of the peaks is seen explicity, where we have placed the target at $s = 22$ and the walker intially at $n_0 = 8$. With a smaller proportion of trajectories set to move in the right direction at $t = 0$ ($\alpha_1 = 0.2$), the periodic case has a large peak at short time, which correspond to the larger fraction of trajectories that move towards the target via the left boundary. The smaller peak at later times is due instead to those walker paths that first headed right. In contrast, with a reflecting boundary at $n = 1$ we do not see a peak until those trajectories that initially headed right reach the target, with a second smaller peak appearing later once the trajectories initially travelling left are reflected back from $n = 1$. In contrast, we observe a very different dynamics when we weigh heavily the walker trajectories so that the majority starts moving right ($\alpha_1 = 0.99$). In such a case we see far less deviation between the two boundary conditions as most persistent trajectories do not encounter the left boundary. We note also that the oscillatory behaviour at short times seen in panels (a) and (c) is a simple consequence of a low sojourn probability as in $c = 0$ limit, one creates parity issues [70]. While here, we are away from this limit, with a low c in short times the chance of being on an even site at even times (given an even initial condition) is still higher. The oscillations dampen with time as the probability of undertaking a sojourn (which breaks the parity) increases.

We now turn our attention to the periodic square lattice and study the probability that the walker reaches a site for the first time moving in a specific direction, and we call this quantity the *directional* first-passage probability. This may be useful in a context where the target is only visible from a certain direction and is obtained by placing a target in only one specific state in a lattice site. We show, in Fig. 5(a), the cases in which the walker reaches the target travelling in each of the four directions. We note that the directional first-passage is a normalised probability distribution as it does not exclude trajectories that first reach the target via an alternate direction. One may ask for the probability of reaching a site for the first time travelling in a specific direction conditioned on the walker having not first reached for the first time from any other direction via the splitting probability in Eq. (23).

With the initial condition at site $\boldsymbol{n}_0 = (4, 2)$, to reach $\boldsymbol{s} = (7, 3)$ for the first time at $t = 4$ or $t = 5$, the walker has to enter the site travelling either North or West. However, travelling West gives a higher directional first-passage at these times because the walker travelling North into the target at $t = 4$ must have made a left-hand turn

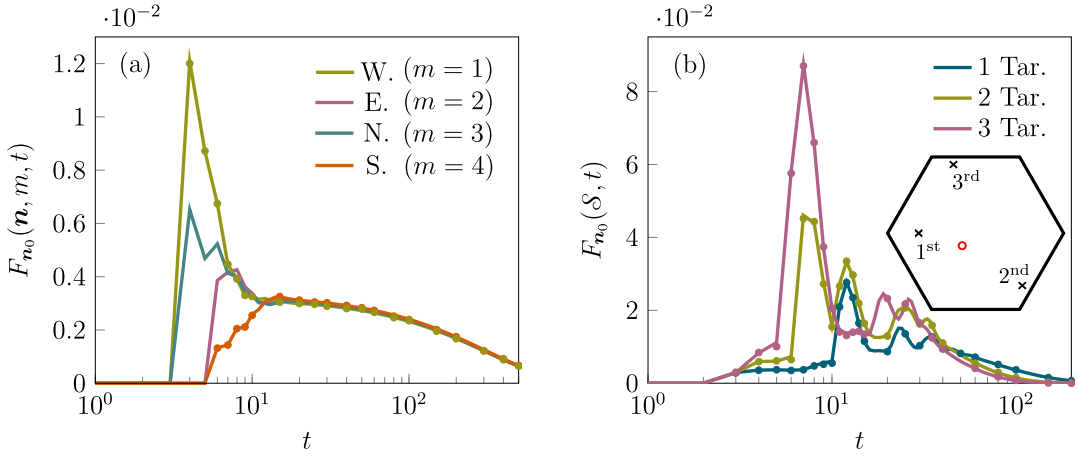

Figure 5. (Colour Online). First-passage probabilities of correlated random walks in two-dimensional periodic domains. In panel (a), through a numerical inversion of Eq. (24), we plot the directional first-passage probability for each of the four movement directions in a square periodic lattice of length $N = 8$ to a single site at $\boldsymbol{s} = (7, 3)$. For example, in order to reach $(\boldsymbol{s}, m_{_s} = 1)$ the walker has to travel West, to reach $(\boldsymbol{s}, m_{_s} = 3)$ the walker has to travel North, etc. The initial condition is at $\boldsymbol{n}_0 = (4, 2)$ with equal probability to move in any direction and with $f = 0.42$, $b = 0.04$ and $\ell = 0.18$. Panel (b) depicts results on a hexagonal lattice and shows, via a numerical inversion of Eq. (22), the first-passage probability to a set $\mathcal{S}$ of one, two, and three targets in a periodic hexagon of circumradius $R = 4$ ($\Omega = 61$) at locations $\boldsymbol{s}_1 = (-3, 3, 0)$, $\boldsymbol{s}_2 = (4, -1, -3)$ and $\boldsymbol{s}_3 = (-3, -1, 4)$, which we add sequentially starting from $\boldsymbol{s}_1$. Since the walker can enter from any direction, all the internal states in $\boldsymbol{s}_i$ are targets. The initial condition in this case is just off centre at $\boldsymbol{n}_0 = (0, 1, -1)$ and $f = 0.80$, $b = 0.02$, $\ell = 0.01$. The approximate location within the domain of the initial condition and target sites are shown via the schematic in the inset, with the initial condition a red open circle and the targets shown with crosses. Dots in (a) and (b) are the result of $5 \cdot 10^6$ and 10^6 stochastic simulations, respectively.

from $\boldsymbol{n} = (7, 2)$ at the preceding time. In contrast, to access the site travelling West at an identical time, the walker has three possible trajectories. After $t = 4$, the West directional first-passage probability sees a sharp decrease, which is a consequence of this timescale being dominated by unlikely trajectories that have had to make a sojourn or an even number of backtracks between the intial condition and the target. Thus, it is here that the Eastern directional first-passage becomes more likely as this timescale coincides with the time in which the Eastern travelling persistent trajectories are able to reach the target.

To analyse an example with multiple absorbing targets (Fig. 5(b)), we consider the hexagonal lattice and place the walker initially in the site $\boldsymbol{n}_0 = (0, 1, -1)$, just to the South-West of the centre of the domain, with uniform initial weighting $\alpha_i = 1/6$ for $i = 1, ..., 6$. We place three targets, the first to the West of the initial condition, the second to the South-East and the third to the North (see the caption of Fig. 5 for the exact coordinates). Since the walker can enter any target via all six directions, the three target case requires 18 target states.

The sustained oscillations, which have only been seen in a small number of systems, including quantum walks [71], biased random walks in hexagonal domains [69] and other non-Markov systems [72] are the natural, higher-dimensional analogue of the bimodality seen in the one-dimensional systems, where again, the peaks correspond to the timescales for which the walker moves away from the target as well as those trajectories that miss the target and must travel round the entire domain. Naturally, as the indirect trajectories take over and more and more trajectories reach the targets, the oscillations dampen and decay to zero [69].

While the multi-modal dynamics is present with one, two and three targets, the placement of targets has a strong effect on the height and location of the peaks. In Fig. 5(c), since the initial condition is slightly off-centered, the high persistence of the walker means the first target (placed directly along the horizontal circumradius) is likely bypassed leading to low search success until a trajectory, which first set off in the opposite direction traverses the boundary. When a second and third target are added just away from the circumradius, the shift imposed by the boundary condition aids the persistent walker in exploring new sections of the domain, which leads to the emergence of the large peak in the two and three target cases. Finally, the third target then kills the second peak since the placement of the third target blocks the route many persistent trajectories took to $\boldsymbol{s}_1$, subsequently increasing the height of the first peak.

6. Summary Statistics and the Mean First-Passage Time

With the generating function of the first-passage time distribution to multiple targets, it becomes an algebraic exercise to extract the n^{th} moments, and in particular its first moment, the mean first-passage time (MFPT), $\mathcal{F}_{\boldsymbol{n_0}\to\{\mathcal{S}\}} = \left.\frac{\partial \widetilde{F}_{\boldsymbol{n_0}}(\mathcal{S},z)}{\partial z}\right|_{z=1}$.

When the initial condition is uniformly distributed across the site, the structure of Eq. (22) is very similar to the Markov first-passage expression for multiple targets [63], and one differentiates $\widetilde{F}_{n_0}(\mathcal{S},z)$ to find

$$\mathcal{F}_{\boldsymbol{n_0}\to\{\mathcal{S}\}} = \frac{\det[\mathbb{T}_0]}{\det[\mathbb{T}_1]-\det[\mathbb{T}]}. \tag{26}$$

The matrices in Eq. (26) are made up of the MFPT between localised sites $\mathcal{F}_{\boldsymbol{n}_0,m_0\to\boldsymbol{s}_i,m_{\boldsymbol{s}_i}}$. More precisely, $\mathbb{T}_{i,i}=0$, $\mathbb{T}_{i,k}=\mathcal{F}_{\boldsymbol{s}_k,m_{\boldsymbol{s}_k}\to\boldsymbol{s}_i,m_{\boldsymbol{s}_i}}$ $(i\neq k)$, $\mathbb{T}_{0_{i,k}}=\mathbb{T}_{i,k}-(2d)^{-1}\sum_{j=1}^{2d}\mathcal{F}_{\boldsymbol{n}_0,m_{0_j}\to\boldsymbol{s}_i,m_{\boldsymbol{s}_i}}$ and $\mathbb{T}_{1_{i,k}}=\mathbb{T}_{i,k}-1$. To find these quantities one evaluates expressions of the form $\mathcal{F}_{\boldsymbol{n}_0,m_0\to\boldsymbol{s}_i,m_{\boldsymbol{s}_i}} = \frac{\partial}{\partial z}\left.\frac{\widetilde{P}_{\boldsymbol{n}_0,m_0}(\boldsymbol{s},m_{\boldsymbol{s}},z)}{\widetilde{P}_{\boldsymbol{s},m_{\boldsymbol{s}}}(\boldsymbol{s},m_{\boldsymbol{s}},z)}\right|_{z=1}$, and we give details and explicit quantities in Sec. VIII of ref. [41]. Performing a summation of Eq. (26) over $\boldsymbol{n}_0$ yields the global mean first-passage time (GMFPT) [35], which we denote as $\mathcal{G}_{\{\mathcal{S}\}}$. In such a case, one replaces $\mathbb{T}_0$ with $\mathbb{G}$ where $\mathbb{G}_{i,j}=\mathbb{T}_{i,j}-(2dN)^{-1}\sum_{\boldsymbol{n}_0}\sum_{j=1}^{2d}\mathcal{F}_{\boldsymbol{n}_0,m_{0_j}\to\boldsymbol{s}_i,m_{\boldsymbol{s}_i}}$, while $\mathbb{T}$ and $\mathbb{T}_1$ are unaffected by the summation. We discuss this quantity further in ref. [41].

In Fig. 6(a), we plot the MFPT for anti-persistent walkers ($f<b$) as a function of f, and a given b. The increase of f has two effects on the walker's ability to spread, namely

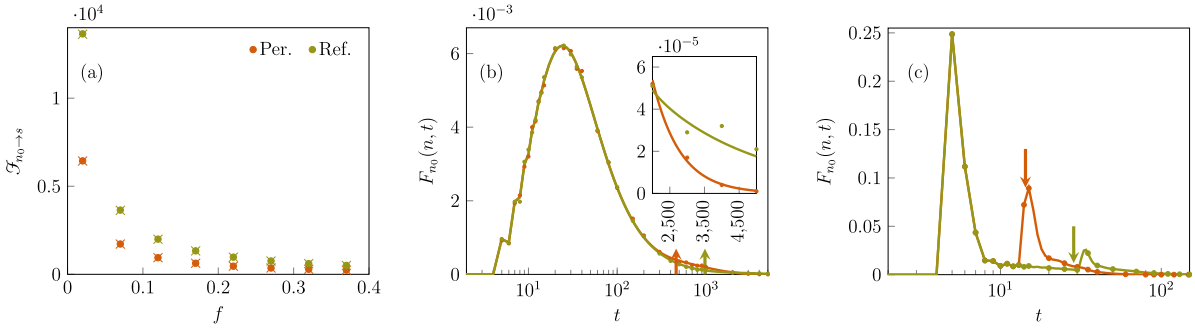

Figure 6. (Colour Online). First-passage probabilities to a single target site and their related mean first-passage times in one-dimensional lattices with periodic (orange) and reflecting (green) boundary conditions. The meaning of the colours, given explicitly in the legend of panel (a), extends over all three plots. In panel (a) we study the MFPT in an $N = 35$ lattice for a walker starting at $n_0 = 30$ with equal weighting of the states in the anti-persistent regime ($b > f$) with the target at $N = s$, by fixing $b = 0.6$ and varying f. Dots represent Eq. (26) evaluated with Eq. (S74) of ref. [41], for the periodic lattice, and Eq. (S75) of ref. [41], for the reflecting lattice. Crosses represent the result of 10^6 stochastic simulations. For the same domain and initial conditions, panel (b) shows the full first-passage probability when $f = 0.22$ and $b = 0.6$. The solid lines are a numerical inversion of Eq. (24), the dots are the result of 10^6 stochastic simulations and the corresponding MFPTs are shown with the arrows. The inset of panel (b) is a blown-up look at the first-passage probabilities in the tails for $t \in [2000, 5000]$. Panel (c) displays the first-passage probability in the persistent regime ($f = 0.86$, $b = 0.06$) where $N = s = 19$ and $n_0 = 14$. Solid lines are generated from the numerical inversion of Eq. (24), the dots are obtained from 10^6 stochastic simulations and the arrows indicate the MFPT.

it decreases both the chance of a sojourn and the probability of turning backwards. This leads to an exponential decrease in the mean search time as the dynamics approaches the diffusive regime. Even though the target is placed only five lattice sites away from the initial condition, the walker takes, on average, 13651 time steps to complete its search in the strong anti-persistent regime ($f = 0.02$). This is due to, in part, those trajectories that have moved far from the target and subsequently have got 'stuck' in cycles of constant backtracking.

It is in panel (b) that one further sees the effect of those trajectories that get stuck far from the target as we display the first-passage probability in another anti-persistent regime where ($f = 0.22$, $b = 0.6$). Since, the initial condition is close to the target and the exploration is extremely slow, there is little difference between periodic and reflecting domains at short and intermediate times. Differences surface at long times since in the periodic domain those walkers that have explored the domain in its entirety may find a short route back to the target, while in the reflective domain walkers are forced to travel back the whole length of the domain. It is these trajectories that contribute to longer tails in the first-passage probability and subsequently the larger MFPT in the reflective case. We note that, similarly to the persistent case, the local minima (and subsequent kinks) seen at short times is again due to the low sojourn probability making

the probability of a first-passage event at even times lower.

Figure 6(c) draws attention to the importance of studying the entire first-hitting distribution in the presence of persistent motion ($f > b$). When first-passage processes display multiple peaks in their time-dependent probability, the MFPT may in fact provide misleading values of the time it takes to hit a target. An extreme example is the ballistic limit, which has two distinct and narrowly defined hitting times given at, for example, $\mathcal{F}^{(r_s)}_{n_0\to s} = s - 1$ ($s > n_0$), $\mathcal{F}^{(r_s)}_{n_0\to s} = N - s$ ($s < n_0$) (for $\alpha_1 = \alpha_2$). In such a case the MFPT would give a temporal value in between the two during which the probability of a first-passage event is identically zero. As shown in panel (c), this aspect may also appear away from the ballistic limit, in the regime of high persistence.

7. Iterative Procedure and Comparison Between Reflective Interactions

In the preceding sections we have exploited the analytical expressions of propagator generating functions. For the cases in which propagators are not known in closed form we present an iterative procedure to find the first-passage probability. While the procedure is valid in arbitrary dimensions, for notational ease we present it here explicitly for the one-dimensional case, and use it as a tool to make comparisons between the two forms of reflection mentioned in Sec. 3.2. We differentiate between the two reflections based on whether an interaction with the boundary invokes a reversal in the direction of movement, which we call the 'bouncing' case, or if the movement direction persists, which we call the 'bunching' case (see panels (c) and (d) in Fig. 1 for pictorial comparison). For an in depth appreciation of the differences between the two boundary conditions we also compare here the occupation probability and the mean square displacement (MSD) in the two cases.

We begin by rewriting the Master equation, Eq. (2), for a finite system using transition matrices that describe the possible movement between lattice sites and link the different internal states. In other words we represent spatial jumps for which the internal state does not change as well as those for which changes between internal states occur. Noting that the probability across the entire site is given by $\boldsymbol{P}_{n_0}(t) = \boldsymbol{P}_{n_0}(1,t)+\boldsymbol{P}_{n_0}(2,t)$, where $\boldsymbol{P}_{n_0}(1,t)$ is an $N \times 1$ column vector of the occupation probabilities of state 1 in each lattice site at time t, we have the Master equation

$$\begin{aligned}\boldsymbol{P}_{n_0}(1,t+1) &= \mathbb{D}\cdot\boldsymbol{P}_{n_0}(1,t) + \mathbb{E}\cdot\boldsymbol{P}_{n_0}(2,t),\\ \boldsymbol{P}_{n_0}(2,t+1) &= \mathbb{F}\cdot\boldsymbol{P}_{n_0}(1,t) + \mathbb{G}\cdot\boldsymbol{P}_{n_0}(2,t),\end{aligned} \tag{27}$$

where $\mathbb{D}$ represents the transition probabilities from state 1 to state 1, $\mathbb{E}$ from state 2 to state 1, $\mathbb{F}$ from state 1 to state 2 and $\mathbb{G}$ encoding the transitions from state 2 to state 2. Due to the finite space, each matrix is of size $N \times N$ and as each matrix only governs a subset of the movement possibilities, they are spars and have the following forms: $\mathbb{D}_{i,i} = c$, for $i \neq 1, N$, $\mathbb{D}_{i,i+1} = a$ and $\mathbb{D}_{1,1} = \delta + c$, $\mathbb{D}_{N,N} = \sigma + c$; $\mathbb{E}_{i,i+1} = b$ and $\mathbb{E}_{1,1} = \omega$; $\mathbb{F}_{i,i-1} = b$ and $\mathbb{F}_{N,N} = \omega$ and $\mathbb{G}_{i,i-1} = a$ and $\mathbb{G}_{1,1} = \sigma + c$, $\mathbb{G}_{N,N} = \delta + c$, where δ, σ, ω are dependent on the chosen boundary conditions. With initial conditions

$P_{n_0}(n,1,0)=\alpha_1$, $P_{n_0}(n,2,0)=\alpha_2$, that is $\boldsymbol{P}_{n_0}(1,0)=\alpha_1\boldsymbol{e}_{n_0}$ and $\boldsymbol{P}_{n_0}(2,0)=\alpha_2\boldsymbol{e}_{n_0}$, it is an iterative task to find the occupation probability at time t.

For the 'bunched' case, $\delta=b$, $\sigma=a$, $\omega=0$, while for the 'bouncing' case, $\delta=b$, $\omega=a$ and $\sigma=0$. To include absorbing traps one sets the outgoing probabilities of a trap state (s,m_s) as $(1-\rho_{s,m_s})A(s,m_s,n,m)$ where ρ_{s,m_s} is the partial absorption probability at (s,m_s) and with $A(s,m_s,n,m)$ representing the elements of the transition matrix encoding movement out of (s,m_s). As an illustration, consider a trap at site $s=N$ and state $m_s=1$. In such a case we multiply the N^{th} column of $\mathbb{D}$ and $\mathbb{F}$ by $(1-\rho_{N,1})$, and the first-passage is obtained via $F_{n_0}(n,t)=S_{n_0}(t-1)-S_{n_0}(t)$ with $F_{n_0}(n,0)=0$, where $S_{n_0}(t)=\sum_{n=1}^{N}P_{n_0}(n,t)$.

In Fig. 7(a), we plot the occupation probability for the bouncing and bunching reflective boundary conditions at varying time steps with uniform initial weighting $\alpha_1=\alpha_2=1/2$. Even at short times one sees higher probability accumulating at the boundaries in the 'bunched' case, with the asymmetry in heights due to the initial condition being placed slightly to the right. At longer times, with the chance of more boundary interaction, the differences become more stark, which pertains until we recover the expected steady states, i.e., uniform probability for the 'bouncing' case and increased probability at the boundaries for the 'bunched' [24].

In panel (b), we compare the MSD, $\Delta(t)=\langle(n(t)-n_0)^2\rangle$, with $\langle\cdot\rangle$ denoting the ensemble average, of a walker confined between either boundary. In the diffusive limit, both boundary conditions are equivalent, which is confirmed by the identical MSD in this case. However, with increasing persistence one sees striking differences between the MSD after boundary interactions have occurred. As predicted from the continuous space-time equivalent analysis for the bouncing case [73], with high positive correlation the MSD shows oscillatory dynamics. In the ballistic limit, these oscillations persist for all times as the walker is guaranteed to return to its initial condition periodically every N timesteps. However, with non-zero backtracking probability, the MSD displays oscillations at short times, which subsequently decay as the result of the different times at which trajectories return to the starting location. Then, due to the uniform steady state when $b\neq 0$ the MSD eventually saturates to $N^2/12$. In contrast, the bunching case sees a clear maxima before quickly lowering to a saturation value, which is dependent on the level of persistence in the system. Since the shape of the steady state is dependent on the level of persistence in the system (where higher persistence levels leads to larger values of the steady state at the boundary [24]), the MSD saturates at higher value for larger $f-b$ with the maximal displacement remaining for all times in the ballistic limit.

In panels (c) and (d), we study the first-passage and as expected, as we increase the possibility of the walker interacting with the boundary, more differences emerge in the first-passage dynamics. To illustrate, in the fully absorbing case, seen in panel (c), differences in the dynamics emerge only at intermediate times when the 'bouncing' walkers display a much higher second peak compared to the 'bunching' ones as they are allowed to reverse their trajectory back towards the target. Instead, in panel (d), where the target is partially absorbing and away from the boundary, the walker may

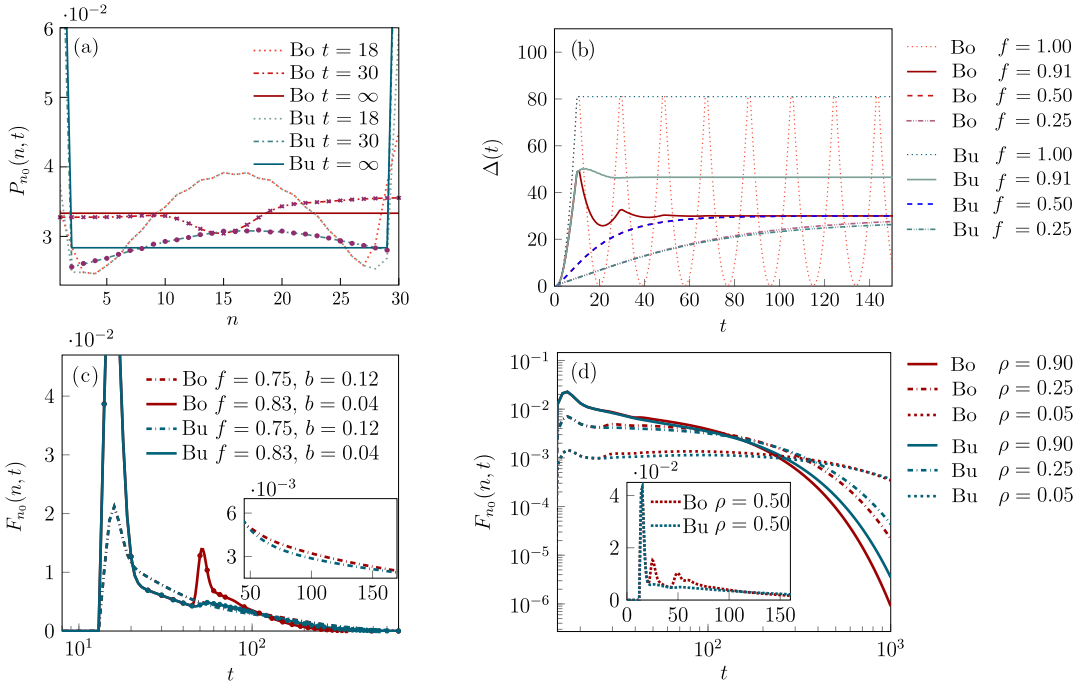

Figure 7. (Colour Online). A comparison of the CRW dynamics between two forms of reflective boundaries, the 'bunching' and 'bouncing' interaction. Across all four panels, the blue-green colours represent the 'bunching' boundary condition, while the red-purple colours represent the 'bouncing' condition. All lines are found via iteratively solving Eq. (27), while crosses are obtained using the analytic propagator in Eq. (10) and all dots are the result of 10^6 stochastic simulations. Panel (a) displays the occupation probability at varying time steps with $f = 0.75$, $b = 0.12$ with $n_0 = 16$ and $N = 30$, and panel (b) shows the MSD for a variety of persistence levels with $(b = 1-f)$ in an $N = 19$ lattice with $n_0 = 10$, that is with the initial condition in the middle of the domain. Panel (c) shows the first passage distribution to site $s = N = 30$, while its inset is a close up of the region of discrepancy between the two boundary conditions when $f = 0.75$, $b = 0.12$. Panel (d) shows the first-passage probability to a partially absorbing target placed at $s = N - 5$ $(N = 30)$, with initial condition $n_0 = 12$ and $f = 0.75$, $b = 0.12$. The inset displays the same type of information, but the movement probabilities are now $f = 0.8$ and $b = 0.04$.

now interact with both the left and right boundary and two timescales emerge where differences occur. The first timescale is due to the trajectories overcoming the target and subsequently being reflected from the right boundary, while the second results from the trajectories that are reflected from the left. Thus, it is the second timescale that is present for all values of ρ (including $\rho = 1$), while the first only emerges for a smaller absorption probability. As we lower ρ further and enter the reaction limited regime (when the timescale for a reaction to occur is much higher than the transport time to reach the target [74]) the two timescales lengthen and begin to merge. For example, when $\rho = 0.05$, one sees a sustained region where the 'bouncing' case has a higher first-passage probability as the walker subject to this boundary condition continuously passes over a target with low adsorption many times.

8. Conclusion

First-passage processes in Markovian LRWs have been studied extensively over the last few years in a multitude of settings [75, 76, 77, 66, 55, 6, 78, 79, 80, 81]. On the other hand, for non-Markovian LRWs a general formalism to derive the first-passage dynamics has been lacking. The simplest non-Markovian LRW extension, the CRW, has received attention, but much of the analysis on first-passage statistics has relied either on time-consuming computational methods [13] or on the global MFPT [36], with very few results known analytically. Here, we have constructed a general formalism to determine the CRW first-passage probability with partially or fully absorbing sites. Furthermore, by deriving closed form expressions for the occupation probability in some instances, we have been able to obtain the first-passage probability generating function analytically. For those cases for which the occupation probability is not known in closed form, we have constructed an iterative procedure to obtain the first-passage probability avoiding the use of computationally burdening stochastic simulations.

While there have been generalisations of renewal processes with continuous variables in the past, e.g., to non-Markovian dynamics [29] and ageing processes [82], they are limited by their analytic tractability, for example, obtaining only moments or asymptotic expansions. Our study instead generalises the renewal formulation in discrete space and time presented by Erdös, Feller and Pollard in 1949 and allows us to link analytically the occupation probability to the first-passage probability for persistent and anti-persistent walks with one or multiple targets. Our formalisms have highlighted the natural appearance of multiple modes in the first-passage dynamics when CRWs with strong persistence occur within finite periodic and reflecting domains. We have also quantified the directional first-passage statistics, that is the first-hitting dynamics based on the direction from which a walker reach a target.

We have obtained analytically the MFPT to one or multiple targets in periodic and reflecting domains, and found a general expression for the GMFPT, which was previously only known for periodic domains [36]. By comparing the first-passage dynamics with its respective MFPT, we find that the multi-modality of the first-passage may lead to cases where the mean actually falls between two modes in a temporal range with a very low chance for a first-passage event to occur.

The theory presented here is rather flexible. It can be extended to biased-correlated random walks [83, 84, 85], may cope with the inclusion of resetting [75, 68] and inert spatial heterogeneities [77] such as permeable barriers [86, 87, 88] or different media [76], and may also be used to account for the dynamics in random environments [89]. We wish also to draw the readers' attention to its applicability to other processes that are conveniently modelled using random walks with internal states such as walks over non-Bravais lattices [55, 35], double-diffusivity [90, 91], dimer migration on a crystalline surface [92, 40] and chromatographic processes [5].

Our findings may also open up the possibility to analyse, the dynamics of active particles in high spatial dimensions [51], encounter statistics [63] of persistent walkers,

exclusion processes [93, 94, 95], cover times [96], record statistics [97] and walks with longer range memory such as the so-called alzheimers [98] and the elephant random walks [99, 100]. Finally, owing to the connection between the two-step CRW and quantum random walks [101], this work in the classical paradigm could help provide tools for its quantum counterpart.

Acknowledgements

The authors acknowledge useful discussions with Toby Kay, Hernán Larralde, Ralf Metzler, and Seeralan Sarvaharman and would like to thank the Isaac Newton Institute for Mathematical Sciences for support and hospitality during the programme *Mathematics of movement: an interdisciplinary approach to mutual challenges in animal ecology and cell biology* when part of the work on this paper was undertaken. This work was supported by: EPSRC grant number EP/R014604/1 and was carried out using the computational facilities of the Advanced Computing Research Centre, University of Bristol - http://www.bris.ac.uk/acrc/. DM acknowledges funding from an Engineering and Physical Sciences Research Council (EPSRC) DTP studentship, while LG acknowledges funding from Biotechnology and Biological Sciences Research Council (BBSRC) Grant No. BB/T012196/1 and the Natural Environment Research Council (NERC) Grant No. NE/W00545X/1.

Appendix A. Reflective Boundary Conditions

To employ the method of images, we note the following. Since a walker moving right (left) must enter into state $m = 1$, ($m = 2$), at the right (left) boundary, it is only the contribution in state $m = 1$ ($m = 2$) that needs to be matched by an image. Then to model the 'bouncing', we invoke a change of state to allow propagation back in the opposing direction by allowing the image of the other state to take over. In Fig. A1, we show this interaction where in the bottom panel, in the succeeding time step, the trajectories that continue left over boundary will be replaced by those in state $m = 1$, indicating the change in direction.

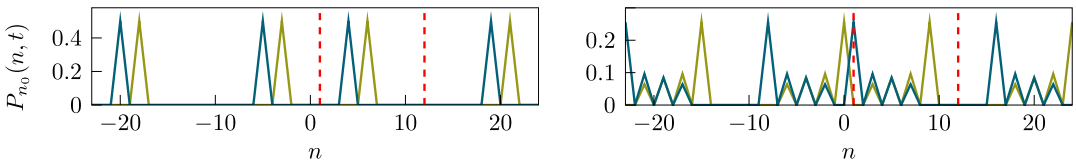

Figure A1. (Colour Online). The interplay between the bounded domain (shown between the two red dotted lines) and the images in three neighbouring domains at timestep $t = 1$ (left) and $t = 4$ (right) found by plotting the scalar expansion of Eq. (10). The occupation probability of state one is shown in green while that of state two in blue. In both panels $f = 0.8$ and $b = 0.2$.

This boundary conditions are generalisable to higher dimensions, e.g. the case

$d = 2$ requires

$$\begin{aligned} P^{(r)}(1, n_2, \{2, 1\}, t) &= P^{(r)}(0, n_2, \{1, 2\}, t), \\ P^{(r)}(N_1, n_2, \{1, 2\}, t) &= P^{(r)}(N_1 + 1, n_2, \{2, 1\}, t), \\ P^{(r)}(n_1, 1, \{4, 3\}, t) &= P^{(r)}(n_1, 0, \{3, 4\}, t), \\ P^{(r)}(n_1, N_2, \{3, 4\}, t) &= P^{(r)}(n_1, N_2 + 1, \{4, 3\}, t), \end{aligned} \tag{A.1}$$

whose sum over the entire site gives, $P^{(r)}(n_1, \{1, N_2\}, t) = P^{(r)}(n_1, \{0, N_2 + 1\}, t)$ and $P^{(r)}(\{1, N_1\}, n_2, t) = P^{(r)}(\{0, N_1 + 1\}, n_2, t)$. This allows one to see that the boundary conditions along either axis are independent of the other, which allows the easy use of the methods of images (see details in the supplementary Material [41]).

Appendix B. The Structure Function

The structure (or characteristic) function is the discrete Fourier transform of the individual step probabilities of the walk [102, 4], which allows for easy inspection of the transport properties of the walk [56]. In systems with no internal degrees of freedom the structure function is scalar, while the inclusion of internal states makes necessary the generalisation to matricial functions of size $\mathfrak{n} \times \mathfrak{n}$, where $\mathfrak{n}$ is the number of internal states.

Presently, the matrix $\boldsymbol{\lambda}\left(\pi\mathcal{N}_{\kappa_1}^{(\gamma)}, ..., \pi\mathcal{N}_{\kappa_d}^{(\gamma)}\right)$ is of size $2d \times 2d$ and has a common structure for all the lattices we have considered here. Namely, the probability of remaining at the same state, i.e. persisting in the direction of the previous movement step or sojourning, is encoded in the diagonal elements, the probability of backtracking is given on the upper and lower diagonal in alternating rows, while all the remaining elements relate to the option of turning laterally. These features are evident in Eq. (4) for the $d = 1$ case, and are seen explicitly also for the two-dimensional hypercubic lattice when we write out the matrix

$$\boldsymbol{\lambda}\left(\pi\mathcal{N}_{\kappa_1}^{(\gamma)}, \pi\mathcal{N}_{\kappa_2}^{(\gamma)}\right) = \begin{bmatrix} fe^{i\pi\mathcal{N}_{\kappa_1}^{(\gamma)}} + c^{(2)} & be^{i\pi\mathcal{N}_{\kappa_1}^{(\gamma)}} & \ell e^{i\pi\mathcal{N}_{\kappa_1}^{(\gamma)}} & \ell e^{i\pi\mathcal{N}_{\kappa_1}^{(\gamma)}} \\ be^{-i\pi\mathcal{N}_{\kappa_1}^{(\gamma)}} & fe^{-i\pi\mathcal{N}_{\kappa_1}^{(\gamma)}} + c^{(2)} & \ell e^{-i\pi\mathcal{N}_{\kappa_1}^{(\gamma)}} & \ell e^{-i\pi\mathcal{N}_{\kappa_1}^{(\gamma)}} \\ \ell e^{i\pi\mathcal{N}_{\kappa_2}^{(\gamma)}} & \ell e^{i\pi\mathcal{N}_{\kappa_2}^{(\gamma)}} & fe^{i\pi\mathcal{N}_{\kappa_2}^{(\gamma)}} + c^{(2)} & be^{i\pi\mathcal{N}_{\kappa_2}^{(\gamma)}} \\ \ell e^{-i\pi\mathcal{N}_{\kappa_2}^{(\gamma)}} & \ell e^{-i\pi\mathcal{N}_{\kappa_2}^{(\gamma)}} & be^{-i\pi\mathcal{N}_{\kappa_2}^{(\gamma)}} & fe^{-i\pi\mathcal{N}_{\kappa_2}^{(\gamma)}} + c^{(2)} \end{bmatrix}. \tag{B.1}$$

As mentioned in the main text (Sec 2), the (i, j)-th element of $\boldsymbol{\lambda}\left(\pi\mathcal{N}_{\kappa_1}^{(\gamma)}, ..., \pi\mathcal{N}_{\kappa_d}^{(\gamma)}\right)$ represents the movement that may occur from state m_j to m_i. The elements of one row, which have identical exponents in the exponentials, represent the one (unique) permissible movement direction of the walker entering the state m_i. For example, $i\pi\mathcal{N}_{\kappa_1}^{(\gamma)}$ in the first row indicates that to enter state m_1, the walker must increase its n_1 coordinate, that is by travelling West, $-i\pi\mathcal{N}_{\kappa_1}^{(\gamma)}$ in the second row shows that to enter m_2 a decrease in the n_1 coordinate occurs by moving East, etc.

From the structure function one may also gain information about the steady state of the system. When $f, b \neq 1$, for hypercubic lattices and hexagonal lattices, in the

limit $t \to \infty$, one has, respectively, $\boldsymbol{\lambda}\left(\pi\mathcal{N}_{\kappa_1}^{(\gamma)},...,\pi\mathcal{N}_{\kappa_d}^{(\gamma)}\right)^t = \mathbf{0}$ and $\boldsymbol{\lambda}^{(\mathcal{H})}\big(\boldsymbol{\kappa}\big)^t = \mathbf{0}$ when $\boldsymbol{\kappa} \neq 0$, while $\lim_{t\to\infty}\boldsymbol{\lambda}\,(0,...,0)^t = (2d)^{-1}\mathbb{J}$, and $\boldsymbol{\lambda}^{(\mathcal{H})}\big(0,0\big)^t = (6)^{-1}\mathbb{J}$, where $\mathbb{J}$ is the all ones matrix. Therefore, $\boldsymbol{P}^{(\gamma)}_{n01,...,n0d}(n_1,...,n_d,t\to\infty) = (2d)^{-1}N^{-d}[1,...,1]^\intercal$ and $\boldsymbol{P}^{(\mathcal{H})}_{\boldsymbol{n}_0}(\boldsymbol{n},t\to\infty) = (6\Omega)^{-1}[1,...,1]^\intercal$, which means that $P^{(\gamma)}_{n01,...,n0d}(n_1,...,n_d,t\to\infty) = N^{-d}$ for $\gamma\in\{p,r\}$ and $P^{(\mathcal{H})}_{n01,n02}(n_1,n_2,t\to\infty) = \Omega^{-1}$ as expected from an irreducible (ergodic) aperiodic finite Markov chain with doubly stochastic transition matrices. When $\gamma = r_s$, that is the squeezed reflecting propagator, in the same limit $\boldsymbol{\lambda}\left(\frac{\pi\kappa}{N-1}\right)^t = \mathbf{0}$ for $\kappa\neq 0$ and $\boldsymbol{\lambda}\,(0)^t = 2^{-1}\mathbb{J}$. Hence, the steady state in this case can be found as $\boldsymbol{P}^{(r_s)}_{n_0}(n,t\to\infty) = (N-1)^{-1}[\alpha_1,\alpha_2]^\intercal$ $(n\neq\{1,N\})$ while $\boldsymbol{P}^{(r_s)}_{n_0}(1,t\to\infty) = \boldsymbol{P}^{(r_s)}_{n_0}(N,t\to\infty) = [2(N-1)]^{-1}[\alpha_1,\alpha_2]^\intercal$. In contrast, when either f or b equals 1, $\boldsymbol{\lambda}\left(\pi\mathcal{N}_{\kappa_1}^{(\gamma)},...,\pi\mathcal{N}_{\kappa_d}^{(\gamma)}\right)$ and $\boldsymbol{\lambda}^{(\mathcal{H})}\big(\boldsymbol{\kappa}\big)$ reduce to generalised permutation matrices, which makes clear that no steady state will be reached.

When $f = 1$, in the periodically bounded domain, one can show that the walker will be at n_0 with certainty every $t = \mathfrak{c}N$ steps ($\mathfrak{c}\in\mathbb{N}\cup\{0\}$), that is the system is a Markov chain with periodicity N. To do so, let us consider the one-dimensional case (the analysis is readily extended to arbitrary dimensions), where $\boldsymbol{\lambda}\left(\frac{2\pi\kappa}{N}\right) = \begin{pmatrix} e^{\frac{2\pi i\kappa}{N}} & 0 \\ 0 & e^{\frac{-2\pi i\kappa}{N}}\end{pmatrix}$. Consequently, $\boldsymbol{P}^{(p)}_{n_0}(n,t) = N^{-1}\sum_{\kappa=0}^{N-1}\exp\left(-\frac{2\pi i\kappa(n-n_0)}{N}\right)\begin{pmatrix} e^{\frac{2\pi i\kappa t}{N}} & 0 \\ 0 & e^{\frac{-2\pi i\kappa t}{N}}\end{pmatrix}\cdot\begin{bmatrix}\alpha_1\\ \alpha_2\end{bmatrix}$. Upon inspection, one clearly sees that when $t = \mathfrak{c}N$ and $n = n_0$, the propagator reduces to $\boldsymbol{P}^{(p)}_{n_0}(n,t) = \begin{bmatrix}\alpha_1 & \alpha_2\end{bmatrix}^\intercal$, such that $P^{(p)}_{n_0}(n_0,\mathfrak{c}N) = 1$.

Appendix C. Defect Technique in Correlated Random Walks

We consider the (unordered) set $\mathcal{S} = \{(\boldsymbol{s}_i,m_{\boldsymbol{s}_i}),...,(\boldsymbol{s}_S,m_{\boldsymbol{s}_S})\}$ of S localised targets. To begin, we write, in arbitrary dimensions and with arbitrary numbers of internal degrees of freedom, the Master equation for the state level dynamics

$$P(\boldsymbol{n},m,t+1) = \sum_{\boldsymbol{n}'}\sum_{m'=1}^{M}\Bigg[A(\boldsymbol{n},m,\boldsymbol{n}',m')P(\boldsymbol{n}',m',t)+ \tag{C.1}$$

$$\sum_{i=1}^{S}\delta_{\boldsymbol{n},\boldsymbol{s}_i}\delta_{m,m_{\boldsymbol{s}_i}}(1-\rho_{\boldsymbol{s}_i,m_{\boldsymbol{s}_i}})A(\boldsymbol{s}_i,m_{\boldsymbol{s}_i},\boldsymbol{n}',m')P(\boldsymbol{n}',m',t)\Bigg], \tag{C.2}$$

where $A(\boldsymbol{n},m,\boldsymbol{n}',m')$ is the transition probability from state $\boldsymbol{n}',m'$ to state $\boldsymbol{n},m$, and $\rho_{\boldsymbol{b}_i,m_{\boldsymbol{b}_i}}$, $(0<\rho_{\boldsymbol{s}_i,m_{\boldsymbol{s}_i}}\leq 1)$ governs the probability of getting absorbed at defect $\boldsymbol{b}_i,m_{\boldsymbol{b}_i}$ where $\rho_{\boldsymbol{s}_i,m_{\boldsymbol{s}_i}} = 1$ represents perfect trapping efficiency at that site. To proceed, one first considers the $\rho_{\boldsymbol{s}_i,m_{\boldsymbol{s}_i}}\neq 1$ case.

Assuming $\sum_{i=1}^{S}\delta_{\boldsymbol{n},\boldsymbol{s}_i}\delta_{m,m_{\boldsymbol{s}_i}}(1-\rho_{\boldsymbol{s}_i,m_{\boldsymbol{s}_i}})A(\boldsymbol{s}_i,m_{\boldsymbol{s}_i},\boldsymbol{n}',m')P(\boldsymbol{n}',m',t)$, for any m, as a given known function the formal solution of Eq. (C.2) is the convolution in space and time of the absorbing propagator with the known terms [63] and proceeding in the

z-domain (i.e., taking the generating function) we find

$$\widetilde{P}^{(a)}(\boldsymbol{n},m,z) = \sum_{\boldsymbol{n}_0'}\sum_{m_0'=1}^{M}\widetilde{P}_{\boldsymbol{n}_0',m_0'}(\boldsymbol{n},m,z)P(\boldsymbol{n},m,0) - z\sum_{\boldsymbol{n}_0'}\sum_{m_0'=1}^{M}\widetilde{P}_{\boldsymbol{n}_0',m_0'}(\boldsymbol{n},m,z)\sum_{i=1}^{S}\rho_{\boldsymbol{s}_i,m_{\boldsymbol{s}_i}}\sum_{\boldsymbol{n}'}\sum_{m'=1}^{M}A(\boldsymbol{s}_i,m_{\boldsymbol{s}_i},\boldsymbol{n}',m')\widetilde{P}(\boldsymbol{n}',m',z). \tag{C.3}$$

By rearranging, and substituting the z-transform of the second term on the RHS of Eq. (C.2) into the second term of Eq. (C.3) the generating function of the formal solution of Eq. (C.2) is found as

$$\widetilde{P}^{(a)}(\boldsymbol{n},m,z) = \sum_{\boldsymbol{n}_0'}\sum_{m_0'=1}^{M}\Bigg[\widetilde{P}_{\boldsymbol{n}_0',m_0'}(\boldsymbol{n},m,z)P(\boldsymbol{n},m,0) + \sum_{i=1}^{S}\frac{\rho_{\boldsymbol{s}_i,m_{\boldsymbol{s}_i}}}{\rho_{\boldsymbol{s}_i,m_{\boldsymbol{s}_i}}-1}\widetilde{P}_{\boldsymbol{s}_i,m_{\boldsymbol{s}_i}}(\boldsymbol{n},m,z)\Big[\widetilde{P}^{(a)}(\boldsymbol{s},m_{\boldsymbol{s}_i},z)-P^{(a)}(\boldsymbol{s},m_{\boldsymbol{s}_i},0)\Big]\Bigg]. \tag{C.4}$$

where we have used $\widetilde{P}_{\boldsymbol{n}_0,m_0}(\boldsymbol{n},m,z)$ to denote any valid (see the main text) defect free propagator.

An initial condition spatially localised over site $\boldsymbol{n}_0$ is given by $P^{(a)}(\boldsymbol{n},0) = \delta_{\boldsymbol{n},\boldsymbol{n}_0}\sum_{m=1}^{M}P^{(a)}(\boldsymbol{n},m,0)$, where the contribution by each state is $P^{(a)}(\boldsymbol{n},m,0) = \delta_{m,m_0}\alpha_{m_0}\left[(1-\rho_{\boldsymbol{s}_i,m_{\boldsymbol{s}_i}})\delta_{(\boldsymbol{n}_0,m_0)\in\mathcal{S}} + \delta_{(\boldsymbol{n}_0,m_0)\notin\mathcal{S}}\right]$. Substitution of this initial condition into Eq. (C.4) leads directly to

$$\widetilde{P}^{(a)}_{\boldsymbol{n}_0,m_0}(\boldsymbol{n},m,z) = \alpha_{m_0}\widetilde{P}_{\boldsymbol{n}_0,m_0}(\boldsymbol{n},m,z) + \sum_{i=1}^{S}\frac{\rho_{\boldsymbol{s}_i,m_{\boldsymbol{s}_i}}}{\rho_{\boldsymbol{s}_i,m_{\boldsymbol{s}_i}}-1}\alpha_{m_{\boldsymbol{s}_i}}\widetilde{P}_{\boldsymbol{s}_i,m_{\boldsymbol{s}_i}}(\boldsymbol{n},m,z)\widetilde{P}^{(a)}_{\boldsymbol{n}_0,m_0}(\boldsymbol{s},m_{\boldsymbol{s}_i},z). \tag{C.5}$$

and following the standard defect technique procedure (see the Supplementary Material [41] for further discussion) i.e., solving via Cramer's rule [63] and taking $\rho_{\boldsymbol{s}_i,m_{\boldsymbol{s}_i}}\to 1$ for all $(\boldsymbol{s}_i,m_{\boldsymbol{s}_i})$, we find

$$\widetilde{P}^{(a)}_{\boldsymbol{n}_0,m_0}(\boldsymbol{n},m,z) = \alpha_{m_0}\widetilde{P}_{\boldsymbol{n}_0,m_0}(\boldsymbol{n},m,z) - \sum_{i=1}^{S}\alpha_{m_{\boldsymbol{s}_i}}\widetilde{P}_{\boldsymbol{s},m_{\boldsymbol{s}_i}}(\boldsymbol{n},m,z)\frac{\det[\mathbb{H}^{(i)}(\boldsymbol{n}_0,m_0,z)]}{\det[\mathbb{H}(z)]}, \tag{C.6}$$

where $\mathbb{H}(z)_{l,k} = \alpha_{m_{\boldsymbol{s}_k}}\widetilde{P}_{\boldsymbol{s}_k,m_{\boldsymbol{s}_k}}(\boldsymbol{s}_l,m_{\boldsymbol{s}_l},z)$, $\mathbb{H}(z)_{k,k} = \alpha_{m_{\boldsymbol{s}_k}}\widetilde{P}_{\boldsymbol{s}_k,m_{\boldsymbol{s}_k}}(\boldsymbol{s}_k,m_{\boldsymbol{s}_k},z)$ and $\mathbb{H}^{(j)}(\boldsymbol{n}_0,m_0,z)$ is the same but with the j^{th} column replaced with $\alpha_{m_0}\left[\widetilde{P}_{\boldsymbol{n}_0,m_0}(\boldsymbol{s}_1,m_{\boldsymbol{s}_1},z),...,\widetilde{P}_{\boldsymbol{n}_0,m_0}(\boldsymbol{s}_S,m_{\boldsymbol{s}_S},z)\right]^{\intercal}$, i.e, they are all known propagators via $\alpha_{m_0}\widetilde{P}_{\boldsymbol{n}_0,m_0}(\boldsymbol{n},m,z) = \alpha_{m_0}\boldsymbol{e}_m^{\intercal}\cdot\widetilde{\boldsymbol{P}}_{\boldsymbol{n}_0}(\boldsymbol{n},z)\cdot\boldsymbol{e}_{m_0}$.

Since $\widetilde{P}^{(a)}_{\boldsymbol{n}_0}(\boldsymbol{n},z) = \sum_{m=1}^{M}\sum_{j=1}^{M}\widetilde{P}^{(a)}_{\boldsymbol{n}_0,m_{0_j}}(\boldsymbol{n},m,z)$, and $\widetilde{P}^{(\gamma)}_{\boldsymbol{n}_0}(\boldsymbol{n},z) = \sum_{m=1}^{M}\sum_{j=1}^{M}\alpha_{m_{0_j}}\widetilde{P}^{(\gamma)}_{\boldsymbol{n}_0,m_{0_j}}(\boldsymbol{n},m,z)$, where there is no α_{m_0} multiplier on the absorbing case as it is already implemented via the initial condition in Eq. (C.5), one may

perform the double summation over both sides of Eq. (C.6) to arrive at Eq. (21) of the main text.

References

[1] R. Nathan, C. T. Monk, R. Arlinghaus, T. Adam, J. Alós, M. Assaf, H. Baktoft, C. E. Beardsworth, M. G. Bertram, A. I. Bijleveld, et al. Big-data approaches lead to an increased understanding of the ecology of animal movement. *Science*, 375(6582):eabg1780, 2022.

[2] E. Meijering, O. Dzyubachyk, and I. Smal. Methods for cell and particle tracking. *Method Enzymol.*, 504:183–200, 2012.

[3] N. Chenouard, I. Smal, F. De Chaumont, M. Maška, I. F. Sbalzarini, Y. Gong, J. Cardinale, C. Carthel, S. Coraluppi, M. Winter, et al. Objective comparison of particle tracking methods. *Nature methods*, 11(3):281–289, 2014.

[4] E. W. Montroll and G. H. Weiss. Random walks on lattices. II. *J. Math. Phys.*, 6(2):167–181, 1965.

[5] G. H. Weiss. *Aspects and applications of the random walk*. Elsevier Science & Technology, 1994.

[6] L. Giuggioli. Exact spatiotemporal dynamics of confined lattice random walks in arbitrary dimensions: A century after Smoluchowski and Pólya. *Phys. Rev. X*, 10:021045, 2020.

[7] P. Mörters and Y. Peres. *Brownian motion*, volume 30. Cambridge University Press, 2010.

[8] P. C. Bressloff. *Stochastic processes in cell biology*, volume 41. Springer, 2014.

[9] V.M. Kenkre and L. Giuggioli. *Theory of the spread of epidemics and movement ecology of animals: an interdisciplinary approach using methodologies of physics and mathematics*. Cambridge University Press, 2021.

[10] A. Bejan and G. W. Merkx. *Constructal theory of social dynamics*. Springer, 2007.

[11] P. Embrechts, C. Klüppelberg, and T. Mikosch. *Modelling extremal events: for insurance and finance*, volume 33. Springer, 2013.

[12] D. Selmeczi, S. Mosler, P. H. Hagedorn, N. B. Larsen, and H. Flyvbjerg. Cell motility as persistent random motion: theories from experiments. *Biophys. J.*, 89(2):912–931, 2005.

[13] B. R. G. Prasad and R. M. Borges. Searching on patch networks using correlated random walks: space usage and optimal foraging predictions using Markov chain models. *J. Theor. Biol.*, 240(2):241–249, 2006.

[14] I. Echeverría-Huarte, A. Garcimartín, R.C. Hidalgo, C. Martín-Gómez, and I. Zuriguel. Estimating density limits for walking pedestrians keeping a safe interpersonal distancing. *Sci. Rep.*, 11(1):1534, 2021.

[15] N. Korabel, G. D. Clemente, D. Han, F. Feldman, T. H. Millard, and T. A. Waigh. Hemocytes in drosophila melanogaster embryos move via heterogeneous anomalous diffusion. *Commun. Phys.*, 5(1):269, 2022.

[16] K. Speckner and M. Weiss. Single-particle tracking reveals anti-persistent subdiffusion in cell extracts. *Entropy*, 23(7):892, 2021.

[17] R. Benelli and M. Weiss. Probing local chromatin dynamics by tracking telomeres. *Biophys. J.*, 121(14):2684–2692, 2022.

[18] A. Gabel and S. Redner. Random walk picture of basketball scoring. *J. Quant. Anal. Sports*, 8(1), 2012.

[19] V.M. Kenkre, V. Ern, and A. Fort. Coherence effects in triplet-exciton transport via time-dependent delayed fluorescence. *Phys. Rev. B*, 28(2):598, 1983.

[20] V.M. Kenkre and Y.M. Wong. Effect of transport coherence on trapping: Quantum-yield calculations for excitons in molecular crystals. *Phys. Rev. B*, 23(8):3748, 1981.

[21] J. Rudnick and G. Gaspari. *Elements of the Random Walk*, volume 1. Cambridge University Press, 2004.

[22] S. Jose, D. Mandal, M. Barma, and K. Ramola. Active random walks in one and two dimensions. *Phys. Rev. E*, 105(6):064103, 2022.

[23] K. Martens, L. Angelani, R. Di Leonardo, and L. Bocquet. Probability distributions for the run-and-tumble bacterial dynamics: An analogy to the lorentz model. *Eur. Phys. J. E*, 35:1–6, 2012.

[24] K. Malakar, V. Jemseena, A. Kundu, K. V. Kumar, S. Sabhapandit, S. N. Majumdar, S. Redner, and A. Dhar. Steady state, relaxation and first-passage properties of a run-and-tumble particle in one-dimension. *J. Stat. Mech-Theory E.*, 2018(4):043215, 2018.

[25] S. Redner. *A guide to first-passage processes*. Cambridge university press, 2001.

[26] R. Metzler, S. Redner, and G. Oshanin. *First-passage phenomena and their applications*, volume 35. World Scientific, 2014.

[27] P. C. Bressloff. Encounter-based model of a run-and-tumble particle. *J. of Stat. Mech. Theory Exp.*, 2022(11):113206, 2022.

[28] L. Angelani. Run-and-tumble particles, telegrapher's equation and absorption problems with partially reflecting boundaries. *J. Phys. A-Math. Theor.*, 48(49):495003, 2015.

[29] T. Guérin, N. Levernier, O. Bénichou, and R. Voituriez. Mean first-passage times of non-Markovian random walkers in confinement. *Nature*, 534(7607):356–359, 2016.

[30] H. Larralde. Transport properties of a two-dimensional "chiral" persistent random walk. *Phys. Rev. E*, 56(5):5004, 1997.

[31] J. Masoliver. Three-dimensional telegrapher's equation and its fractional generalization. *Phys. Rev. E*, 96(2):022101, 2017.

[32] R. Furth. The brownian motion with consideration of the longevity of the direction of movement. *Z. Phys.*, 2:244–256, 1920.

[33] G. I. Taylor. Diffusion by continuous movements. *Proc. London Math. Soc.*, 2(1):196–212, 1922.

[34] H. Larralde. First-passage probabilities and mean number of sites visited by a persistent random walker in one-and two-dimensional lattices. *Phys. Rev. E*, 102(6):062129, 2020.

[35] E. W. Montroll. Random walks on lattices. III. Calculation of first-passage times with application to exciton trapping on photosynthetic units. *J. Math. Phys.*, 10(4):753–765, 1969.

[36] V. Tejedor, R. Voituriez, and O. Bénichou. Optimizing persistent random searches. *Phys. Rev. Lett.*, 108(8):088103, 2012.

[37] H. Shum and E. A. Gaffney. Hydrodynamic analysis of flagellated bacteria swimming in corners of rectangular channels. *Phys. Rev. E*, 92(6):063016, 2015.

[38] N. G. van Kampen. Remarks on non-Markov processes. *Braz. J. Phys.*, 28:90–96, 1998.

[39] J. Masoliver, J. M. Porra, and G. H. Weiss. Solutions of the telegrapher's equation in the presence of traps. *Phys. Rev. A*, 45(4):2222, 1992.

[40] U. Landman and M. F. Shlesinger. Stochastic theory of multistate diffusion in perfect and defective systems. ii. case studies. *Phys. Rev. B*, 19(12):6220, 1979.

[41] See supplementary material for further details on the derivations.

[42] B. D. Hughes. *Random walks and random environments Volume 1: Random Walks*. Clarendon Press Oxford ; New York, 1995.

[43] M. H. Ernst. Random walks with short memory. *J. Stat. Phys.*, 53:191–201, 1988.

[44] C. Bechinger, R. Di Leonardo, H. Löwen, C. Reichhardt, G. Volpe, and G. Volpe. Active particles in complex and crowded environments. *Rev. Mod. Phys.*, 88(4):045006, 2016.

[45] Z. Kalay. Effects of confinement on the statistics of encounter times: exact analytical results for random walks in a partitioned lattice. *J. Phys. A-Math. Theor.*, 45(21):215001, 2012.

[46] J. B. Keller. The scope of the image method. *Commun. Pur. Appl. Math.*, 6(4):505–512, 1953.

[47] J. Masoliver, J. M. Porra, and G. H. Weiss. Solution to the telegrapher's equation in the presence of reflecting and partly reflecting boundaries. *Phys. Rev. E*, 48(2):939, 1993.

[48] E. W. Montroll. Random walks in multidimensional spaces, especially on periodic lattices. *J. Soc. Ind. Appl. Math.*, 4(4):241–260, 1956.

[49] G. Beylkin, C. Kurcz, and L. Monzón. Fast algorithms for Helmholtz Green's functions. *P. Roy. Soc. A-Math. Phy.*, 464(2100):3301–3326, 2008.

[50] S. Chandrasekhar. Stochastic problems in physics and astronomy. *Rev. Mod. Phys.*, 15(1):1,

1943.

[51] K. Proesmans, R. Toral, and C. Van den Broeck. Phase transitions in persistent and run-and-tumble walks. *Physica A Stat.*, 552:121934, 2020.

[52] N. R. Smith, P. Le Doussal, S. N. Majumdar, and G. Schehr. Exact position distribution of a harmonically confined run-and-tumble particle in two dimensions. *Phys. Rev. E*, 106(5):054133, 2022.

[53] M. Miri and H. Stark. Persistent random walk in a honeycomb structure: Light transport in foams. *Phys. Rev. E*, 68(3):031102, 2003.

[54] I. Her. Geometric transformations on the hexagonal grid. *IEEE Trans. Imag. Process.*, 4(9):1213–1222, 1995.

[55] D. Marris, S. Sarvaharman, and L. Giuggioli. Exact spatiotemporal dynamics of lattice random walks in hexagonal and honeycomb domains. *Phys. Rev. E*, 107(5):054139, 2023.

[56] F. Spitzer. *Principles of random walk*, volume 34. SpringerVerlag, second edition, 1976.

[57] H. Larralde and F. Leyvraz. Three-dimensional diffusion with helical persistence. *J. Phys. A-Math. Theor.*, 48(26):265001, 2015.

[58] J. Masoliver, J. M. Porra, and G. H. Weiss. Some two and three-dimensional persistent random walks. *Physica A: Statistical Mechanics and its Applications*, 193(3-4):469–482, 1993.

[59] C. Hargus, J. M. Epstein, and K. K. Mandadapu. Odd diffusivity of chiral random motion. *Phys. Rev. Lett.*, 127(17):178001, 2021.

[60] F. Kümmel, B. Ten Hagen, R. Wittkowski, I. Buttinoni, R. Eichhorn, G. Volpe, H. Löwen, and C. Bechinger. Circular motion of asymmetric self-propelling particles. *Phys. Rev. Lett.*, 110(19):198302, 2013.

[61] I. H. Riedel, K. Kruse, and J. Howard. A self-organized vortex array of hydrodynamically entrained sperm cells. *Science*, 309(5732):300–303, 2005.

[62] P. Fuchter and H. Bloomfield-Gadêlha. The three-dimensional coarse-graining formulation of interacting elastohydrodynamic filaments and multi-body microhydrodynamics. *J. R. Soc. Interface*, 20(202):20230021, 2023.

[63] L. Giuggioli and S. Sarvaharman. Spatio-temporal dynamics of random transmission events: from information sharing to epidemic spread. *J. Phys. A-Math. Theor.*, 55(37):375005, 2022.

[64] J. Abate and W. Whitt. Numerical inversion of probability generating functions. *Oper. Res. Lett.*, 12(4):245–251, 1992.

[65] J. Abate, G. L. Choudhury, and W. Whitt. An introduction to numerical transform inversion and its application to probability models. In *Computational probability*, pages 257–323. Springer, 2000.

[66] S. Sarvaharman and L. Giuggioli. Closed-form solutions to the dynamics of confined biased lattice random walks in arbitrary dimensions. *Phys. Rev. E*, 102(6):062124, 2020.

[67] J. Holhouse and S. Redner. First-passage on disordered intervals. *arXiv preprint arXiv:2307.08879*, 2023.

[68] O. L. Bonomo and A. Pal. First passage under restart for discrete space and time: application to one-dimensional confined lattice random walks. *Phys. Rev. E*, 103(5):052129, 2021.

[69] L. Giuggioli, S. Sarvaharman, D. Das, D. Marris, and T. Kay. Multi-target search in bounded and heterogeneous environments: a lattice random walk perspective. *arXiv preprint arXiv:2311.00464*, 2023.

[70] M. Kac. Random walk and the theory of brownian motion. *Am. Math. Mon.*, 54(7):369–391, 1947.

[71] M. Kulkarni and S. N. Majumdar. First detection probability in quantum resetting via random projective measurements. *arXiv preprint arXiv:2305.15123*, 2023.

[72] T. Verechtchaguina, I.M. Sokolov, and L. Schimansky-Geier. First passage time densities in non-Markovian models with subthreshold oscillations. *Europhys. Lett.*, 73(5):691, 2006.

[73] L. Giuggioli, J.R. Potts, and S. Harris. Predicting oscillatory dynamics in the movement of territorial animals. *J. R. Soc. Interface.*, 9(72):1529–1543, 2012.

[74] V. M. Kenkre and P. Reineker. *Exciton dynamics in molecular crystals and aggregates.* Springer, 2006.

[75] D. Das and L. Giuggioli. Discrete space-time resetting model: Application to first-passage and transmission statistics. *J. Phys. A-Math. Theor.*, 55(42):424004, 2022.

[76] D. Das and L. Giuggioli. Dynamics of lattice random walk within regions composed of different media and interfaces. *J. Stat. Mech-Theory E.*, 2023(1):013201, 2023.

[77] S. Sarvaharman and L. Giuggioli. Particle-environment interactions in arbitrary dimensions: a unifying analytic framework to model diffusion with inert spatial heterogeneities. *Phys. Rev. Res.*, 5(4):043281, 2023.

[78] O. Bénichou and R. Voituriez. From first-passage times of random walks in confinement to geometry-controlled kinetics. *Phys. Rep.*, 539(4):225–284, 2014.

[79] S. Condamin, O. Bénichou, and M. Moreau. First-passage times for random walks in bounded domains. *Phys. Rev. Lett.*, 95(26):260601, 2005.

[80] A. Godec and R. Metzler. First passage time distribution in heterogeneity controlled kinetics: going beyond the mean first passage time. *Sci. Rep-UK*, 6(1):20349, 2016.

[81] A. Godec and R. Metzler. Universal proximity effect in target search kinetics in the few-encounter limit. *Phys. Rev. X*, 6(4):041037, 2016.

[82] J. H. P. Schulz, E. Barkai, and R. Metzler. Aging renewal theory and application to random walks. *Phys. Rev. X*, 4:011028, 2014.

[83] S. Godoy and S. Fujita. Reflection principles for biased correlated walks. simple applications. *J. Math. Phys.*, 33(9):2998–3003, 1992.

[84] V. Rossetto. The one-dimensional asymmetric persistent random walk. *J. Stat. Mech-Theory E.*, 2018(4):043204, 2018.

[85] R. García-Pelayo. Solution of the persistent, biased random walk. *Physica A*, 384(2):143–149, 2007.

[86] T. Kay and L. Giuggioli. Diffusion through permeable interfaces: fundamental equations and their application to first-passage and local time statistics. *Phys. Rev. Res.*, 4(3):L032039, 2022.

[87] P.C. Bressloff. A probabilistic model of diffusion through a semi-permeable barrier. *Proc. R. Soc. A*, 478(2268):20220615, 2022.

[88] T. Kosztołowicz. Random walk in a discrete and continuous system with a thin membrane. *Phys. A: Stat. Mech. Appl.*, 298(3-4):285–296, 2001.

[89] D. Szász and B. Tóth. Persistent random walks in a one-dimensional random environment. *J. Stat. Phys.*, 37(1-2):27–38, 1984.

[90] J. M. Hill. A discrete random walk model for diffusion in media with double diffusivity. *ANZIAM J.*, 22(1):58–74, 1980.

[91] J. M. Hill and B.D. Hughes. On the general random walk formulation for diffusion in media with diffusivities. *ANZIAM J.*, 27(1):73–87, 1985.

[92] U. Landman and M. F. Shlesinger. Stochastic theory of multistate diffusion in perfect and defective systems. i. mathematical formalism. *Phys. Rev. B*, 19(12):6207, 1979.

[93] S. Zhang, A. Chong, and B. D. Hughes. Persistent exclusion processes: Inertia, drift, mixing, and correlation. *Phys. Rev. E*, 100(4):042415, 2019.

[94] E. Teomy and R. Metzler. Transport in exclusion processes with one-step memory: density dependence and optimal acceleration. *J. Phys. A-Math. Theor.*, 52(38):385001, 2019.

[95] E. Gavagnin and C. A. Yates. Modeling persistence of motion in a crowded environment: The diffusive limit of excluding velocity-jump processes. *Phys. Rev. E*, 97(3):032416, 2018.

[96] L. Régnier, M. Dolgushev, S. Redner, and O. Bénichou. Universal exploration dynamics of random walks. *Nat. Comms.*, 14(1):618, 2023.

[97] L. Régnier, M. Dolgushev, and O. Bénichou. Record ages of non-Markovian scale-invariant random walks. *Nat. Commun.*, 14(1):6288, 2023.

[98] J. C. Cressoni, M. A. A. da Silva, and G.M. Viswanathan. Amnestically induced persistence in random walks. *Phys, Rev. Lett.*, 98(7):070603, 2007.

[99] G. M. Schütz and S. Trimper. Elephants can always remember: Exact long-range memory effects in a non-Markovian random walk. *Phys. Rev. E*, 70(4):045101, 2004.

[100] V.M. Kenkre. Analytic formulation, exact solutions, and generalizations of the elephant and the alzheimer random walks. *arXiv preprint arXiv:0708.0034*, 2007.

[101] S. Boettcher, S. Falkner, and R. Portugal. Renormalization group for quantum walks. In *J. Phys. Conf. Ser.*, volume 473, page 012018. IOP Publishing, 2013.

[102] J. Klafter and I. M. Sokolov. *First steps in random walks: from tools to applications*. OUP Oxford, 2011.